A New Look at the Pacific Storm Track Variability: Sensitivity to Tropical SSTs and to Upstream Seeding

ISIDORO ORLANSKI

NOAA/Geophysical Fluid Dynamics Laboratory, Princeton University, Princeton, New Jersey

(Manuscript received 23 March 2004, in final form 23 September 2004)

ABSTRACT

There is a fairly well defined stationary wave and storm track response to El Niño SSTs over the Pacific. In this paper, the case is made that this response is a direct result of increased baroclinicity in the central Pacific and that changes in the stationary wave pattern farther east are primarily forced by changes in these transient eddies. There is also a lot of natural variability that is not associated with El Niño. The paper also stresses the point that much of the variability can be understood as forced by variations in the upstream seeding of the storm track. The question of whether these seeding variations should be thought of as chaotic noise or forced by identifiable mechanisms is not addressed. Thus, the claim is that the storm track variability and its feedback to the quasi-stationary circulation depends on two key parameters: mid-Pacific baroclinicity, controlled by SSTs, and the strength of the upstream seeding.

The approach is to first examine the effect of storm track seeding by waves entering from the Asian continent during normal years (non-ENSO years). The results show that two mechanisms operate to distribute eddy energy along the storm track: downstream development and baroclinic development. The large effect on baroclinic development at the storm track entrance results from a combination of factors: surface baroclinicity, land–sea contrast, and strong moist fluxes from the western subtropics. Experiments show that sensitivity to the seeding amplitude is large. The larger the seeding amplitude, the closer the more intense baroclinic waves flux energy downstream to upper-level waves. These barotropic waves tend to break anticyclonically and produce a ridge in the eastern Pacific.

Sensitivity to SST anomalies shows qualitative and quantitative similarity with the observed anomalies. Simulations show increased mid-Pacific baroclinicity because stronger convection in the midtropical Pacific enhances a large pool of warm air over the entire mideastern subtropical ocean. Waves with sources at the storm track entrance break anticyclonically and produce the ridge in the eastern Pacific. On the other hand, baroclinic waves generated or regenerated in the mid-Pacific tend to break cyclonically, produce a trough tendency, and reduce the eastern ridge amplitude in the Pacific–North American (PNA) sector.

These results strongly suggest that

1) the variability of the quasi-permanent circulation indeed could be produced by the high-frequency eddy feedback, and
2) two mechanisms are primarily responsible for the forcing of the quasi-permanent circulation: *downstream development* from the western Pacific and the anomalous *baroclinicity in the mideastern Pacific.*

The intensity of these counteracting forcings gives the different flavors of the El Niño response over the PNA region. Regardless of the SST anomaly strength, the PNA patterns seem unique but obviously have different intensities.

1. Introduction

Despite the large number of articles devoted to the role of tropical SSTs in the variability of the northern winter Pacific storm track, the topic remains controversial (see Hoerling and Kumar 2002, hereafter HK02, for an extended reference). HK02 presents a very complete discussion on the extratropical response variability over the Pacific–North America region (PNA) and its relation with tropical SSTs, particularly with ENSO variability. They concluded that, clearly, the existence of a teleconnection pattern forced by changes in tropical SSTs is associated with the El Niño–Southern Oscillation (ENSO). However, they also noted that variations in the extratropical atmospheric response to different El Niños are quite large.

It is more or less an accepted fact that the year-to-year PNA sector variability explained by ENSO is indeed limited by the intrinsic atmospheric variability. Observed seasonal anomalies during different El Niños are often distinct from each other, though contrary in-

Corresponding author address: Dr. Isidoro Orlanski, NOAA/GFDL, Princeton University, Forrestal Campus, Princeton, NJ 08542.
E-mail: isidoro.orlanski@noaa.gov

terpretations have been offered. Madden (1976) proposed that the observed monthly sea level pressure variability is due to the internal atmospheric variations attributable to daily weather fluctuations and is not caused by sensitivity to boundary forcing. This argument has been supported by general circulation model results (Geisler et al. 1985; Kumar and Hoerling 1997) that find only a weak extratropical sensitivity to changes in tropical Pacific SSTs from event to event.

A contradictory argument, offered by Palmer and Owen (1986), suggests that the inter–El Niño differences in the extratropical seasonal anomaly can be explained by SST variations. This supports the contention that a substantial signal exists in the extratropics that varies from one ENSO event to another (Trenberth 1993). HK02 analyzed the results of a large number of ensemble atmospheric climate simulations forced with the modern record of interannually varying tropical forcing. They concluded that the observed estimate of the fraction of year-to-year PNA sector variability explained by ENSO is indeed limited by the intrinsic atmospheric variability. Furthermore, as they mention, much of the ENSO response manifests itself as a single spatial pattern. Other patterns were identified; however, they contributed a very small signal over the PNA sector as a whole.

Although the tropical forcing origin seems clear, the so-called atmospheric variability is considerably more obscure. Simmons et al. (1983) suggested that low-frequency barotropic waves, of 30–50-day periods, generated by barotropic instability could be the cause determining the response to anomalous boundary forcing, such as tropical SSTs. We know that high-frequency baroclinic eddies can play a significant role in shaping the large-scale variability of the Pacific storm track (Held et al. 1989; Lau and Nath 1991; Hoerling and Ting 1994; Orlanski 1998; Chang et al. 2002; among others). Moreover, Orlanski (1998), analyzing the barotropic forcing exerted by baroclinic eddies over two ENSO cycles, suggested that the quasi-stationary response of the upper-level heights has strong similarities with the observed PNA pattern. More recently, Orlanski (2003) found a very suggestive result that the intensity of high-frequency low-level baroclinic waves can force the upper-level waves such that for low-amplitude forcing, the upper-level waves break anticyclonically and move the jet poleward. As the forcing increases, this mechanism intensifies and stronger low-level eddies push the upper-level jet farther north. Furthermore, eddy intensification produces a drastic change in upper-level wave breaking. Waves break cyclonically and consequently, the jet is pushed equatorward. Since this behavior shift depends on reaching a critical energy level and the horizontal scale of the waves, short baroclinic waves frequently reach the threshold and break cyclonically. Longer waves require much more energy to produce the shift. Thus, we can conclude that the bifurcation of eddy life cycles has a bearing on the interannual variability of storm tracks.

By contrast, in non–El Niño years, baroclinic development enhances waves entering from eastern Asia to the Pacific storm track entrance: the waves disperse by downstream energy flux and develop a more barotropic upper-level wave since the mid-Pacific region is depleted of most of its baroclinicity (Chang and Orlanski 1993). Consequently, the barotropic waves break anticyclonically in the eastern Pacific. In El Niño years, as convective regions move to the mid-Pacific, enhanced baroclinicity in the subtropics could enhance baroclinic development farther eastward and support more intense, shorter waves that eventually will break cyclonically and maintain the subtropical jet eastward. Given the large amount of work on this topic (HK02; Kushnir et al. 2002; among others), it seems clear that although the mechanisms are not well understood, the sensitivity of the extratropical response to anomalous tropical SSTs has considerable variability, and the combined role of boundary forcing (through tropical SSTs) and internal atmospheric variability appear to be responsible for such behavior.

The work presented here is quite distinct from the many articles written on the subject. First, a high-resolution nonhydrostatic model with explicit convection is used to simulate the Pacific storm track and its sensitivity to tropical SSTs and natural variability. The experiments are designed to treat the natural variability and the effect of tropical SST anomalies independently. The premise is simple: assume that most of the variability is connected in some way to the high-frequency eddy activity in the storm track (Orlanski 1998, 2003). Then, our goal is to assess

- how much the natural variability, measured as high-frequency waves entering the western Pacific storm track, can affect the response in the storm track;
- how tropical anomalous SSTs can produce the well-known response in the PNA region; and
- how the natural variability interferes with the surface boundary forcing to provide great variability in the storm track response in the PNA region.

The model and experimental setting are described in section 2. The control solution is presented in section 3 and changes due to natural variability are discussed in section 4. Details of the storm track response to tropical heating anomalies are shown in section 5. Finally, the summary and conclusions are presented in section 6.

2. Model and methodology

The solutions were obtained by integrating a compressible nonhydrostatic high-resolution ZETAC[1]

[1] The ZETAC model (developed by Dr. Steve Garner) is written using the Geophysical Fluid Dynamics Laboratory (GFDL) Flexible Modeling System (FMS).

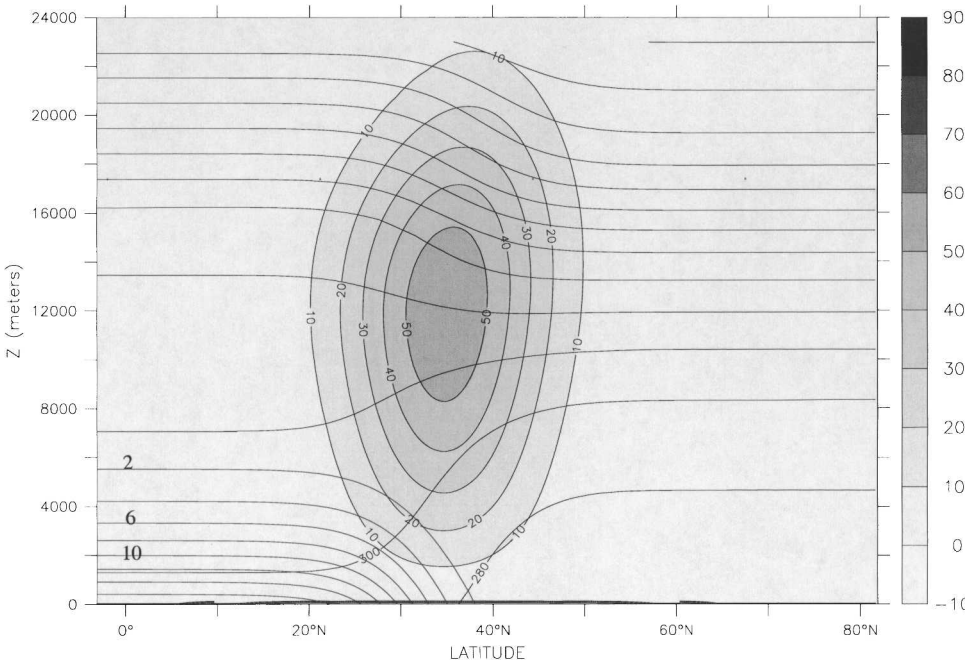

FIG. 1. Cross section of the zonal jet, potential temperature, and water vapor (contour interval is 2 g kg^{-1}; the maximum contour at the surface in the Tropics is 18 g kg^{-1}) forced at the entrance of the storm track in the western Pacific Ocean.

model (9- and 18-km horizontal resolutions in the storm track region, see the appendix). The simulation area encompasses the entire North Pacific Ocean from 3°S to 82.5°N, 120°E to 85°W. Other model characteristics include a terrain-following coordinate that extends from the surface to around 25-km height and an explicit moist convection with a simple Kessler microphysics parameterization. The regional model is forced only by the SST and prescribed inflow conditions at the western boundary (see the appendix). An inflow condition, an idealized climatological jet as shown in Fig. 1, defines the storm track entrance. Prescribing a SST as shown in Fig. 2 defines the lower ocean boundary forcing. The model is integrated for 220 days and analysis of the last 50 days provides the control solution. Note that air in the upper atmosphere crosses the entire basin in around 4 days.

As mentioned, we will evaluate two independent effects: the natural variability and the tropical SST anomaly affecting the storm track response in the PNA sector. Accordingly, we perform sensitivity experiments by initializing different cases at day 140 of the control, run the solution to 220 days and compare the last 50 days of each solution to the control. Testing SST sensitivity is rather simple. Using the SST shown in Fig. 2 we include an anomaly in the Tropics that mimics the gross features of El Niño SSTs (slightly different SSTs have been used to reflect moderate and strong El Niño events). Regarding the natural variability evaluation, we assume that most of the variability is generated by wave activity from Asia at the storm track entrance. Therefore, we nudge the zonal and meridional velocities at the western boundary with an upper-level wave in which the amplitude and frequency are random (see the appendix). The vertical and meridional form of the wave maker is similar to an upper-level barotropic wave, similar in shape to the prescribed jet. The forced amplitude standard deviation is set to values close to the observed values for winter conditions. Two standard deviation values were used to characterize the wave noise, 5 (*moderate*) and 8 m s^{-1} (*strong*); the random period fluctuated from 3 to 5 days (there is a lookup table for random periods and amplitudes. A selected oscillation maintains its characteristics until its period iscomplete; then a new oscillation is selected that has a different random period and amplitude). These rather high-frequency forcings were intentional to ascertain whether any low-frequency response in the simulation originated from a high-frequency forcing. More details on the random forcing appear in the next section. No other boundary or interior forcing has been applied. Given the assumption that considerable feedback is from the high-frequency eddies that modify the large-scale flow in the storm track, we want the model to freely determine its large-scale circulation rather than be forced to a prescribed one.

3. The control solution

Figure 3 shows the time-averaged variables of the Control solution. The time mean distribution of these

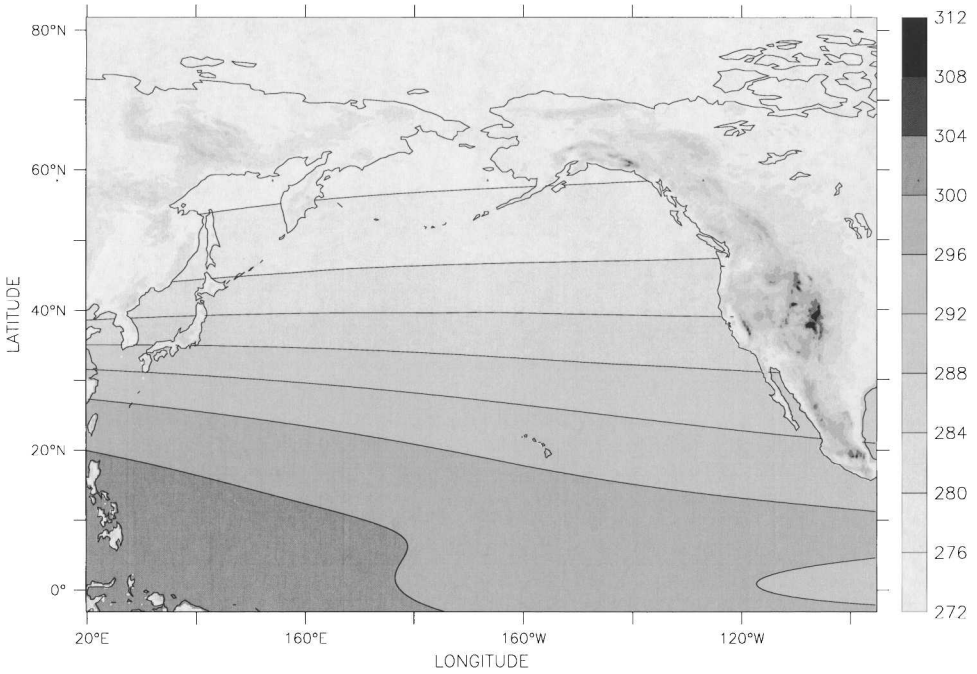

FIG. 2. Sea surface temperature used for the Control simulation. Larger meridional temperature gradients and higher equatorial temperatures are seen in the western region; this is similar to the climatological state (contour interval is 4°C; the dark gray pool in the western Tropics is about 304°C).

quantities seems very realistic. The zonal component of the wind at 8900 m (upper-left panel) shows the jet intensification in the western Pacific and the poleward deflection in the eastern Pacific. It is a classical picture of the trough–ridge associated with the storm track (Orlanski 1998); the magnitude and poleward displacement of the subtropical jet seem very realistic for winter conditions. The other fields also seem very well resolved, especially the intensification of the moist thermodynamic variables in the tropical western region. The remaining panels show the surface potential temperature (lower left), the pressure deviations from the zonal average (upper right), and water vapor (lower right). The precipitation is coincident with the tongue of warm surface temperatures in the western equatorial ocean. This indicates that the idealized simulation captures the characteristics of the tropical convection reasonably well. The time mean pressure perturbation of the zonal pressure (upper-right panel) displays a trough in the mid–Pacific Ocean bounded by two ridges with the most intense ridge over the PNA sector. However, notice that, although the ridge position correlates well with observations, the observations also show that the trough starts at the storm track entrance and extends east of the date line. This trough actually is generated by two distinct processes: the Tibetan Plateau and the baroclinic eddy feedback. The large orography produces a trough to the lee of the plateau extending to the western Pacific Ocean (Held et al. 2002), and the feedback from baroclinic eddies produces a trough around the middle of the storm track (Lau and Nath 1991; Orlanski 1998). The Tibetan Plateau effect is certainly missing from our experimental design but it does not detract from the generalities of the conclusions. The downstream intensity of the trough displayed in the figure will be discussed shortly.

Figure 4 shows the variance of the upper-level meridional velocity for the December–January climatology of the National Centers for Environmental Prediction–National Center for Atmospheric Research (NCEP–NCAR) reanalysis. The middle panel shows the time-averaged variance for the Control with moderate seeding (this will be the reference solution used throughout the paper), and at the bottom, a solution with conditions similar to the Control but with strong seeding on the western boundary. Occasionally throughout the paper we will show some climatology from the NCEP–NCAR reanalysis similar to that shown in Fig. 4. We need to stress the fact that neither the mean flow nor the SSTs, in the simulations, are from real data; only the topography is real, and showing a comparison with climatology could be misleading. However, since this paper relies heavily on the intensity of the high-frequency baroclinic eddies, it would be instructive to show the observed variance and see that we are in the realm of realistic simulations. Actually, the similarities and energy levels are quite striking. An in-depth discussion on the upstream seeding follows.

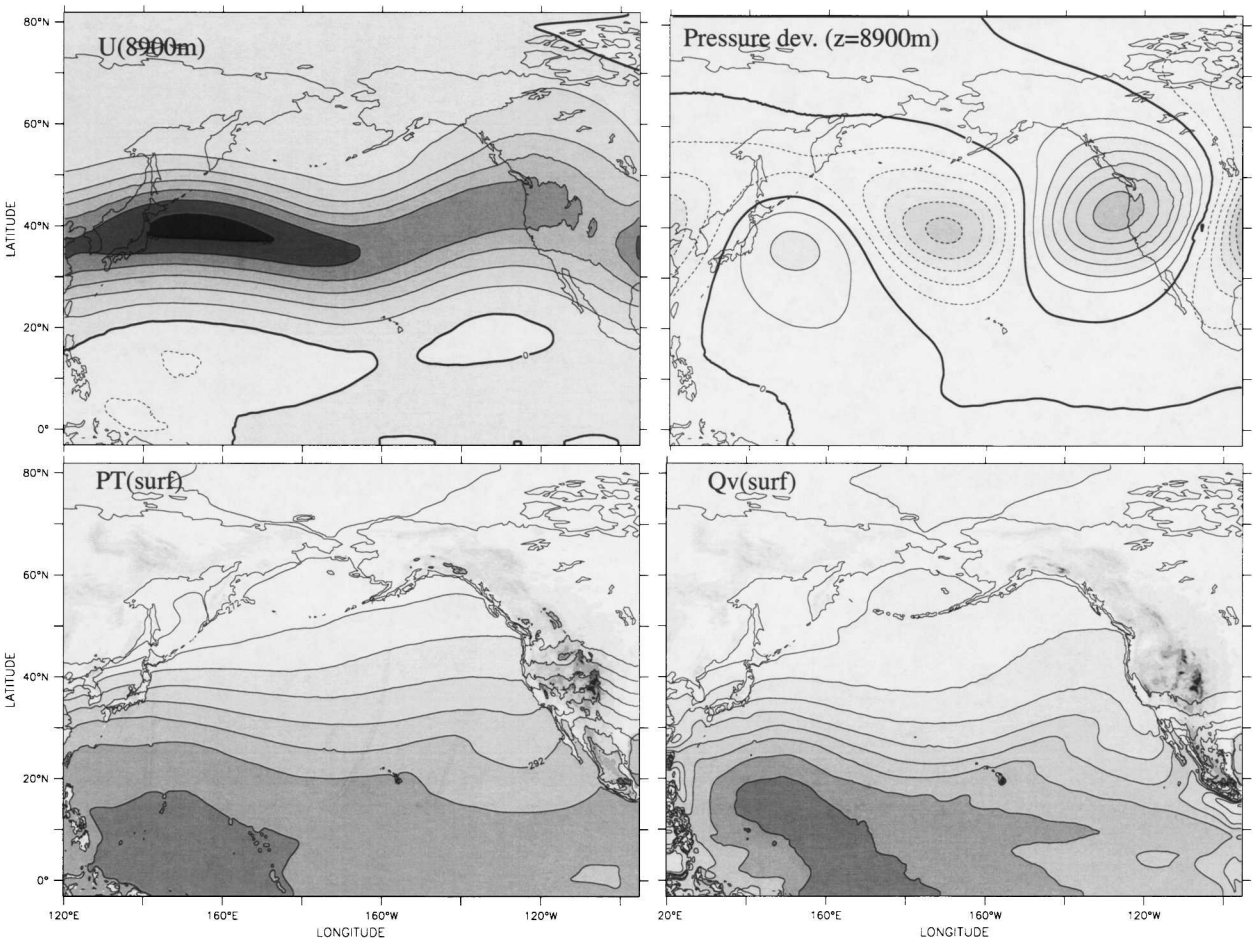

FIG. 3. The time-averaged fields (50 days) for the Control solution (moderate seeding). (upper left) Zonal wind at the upper levels [contour interval (CI) = 10 m s^{-1}]. (upper right) Pressure deviation of the zonally averaged mean pressure (CI = 2 hPa; the maximum over the eastern Pacific is 12 hPa). (lower left) Surface potential temperature (CI = 4°C) and (lower right) surface water vapor (CI = 0.002 g kg^{-1}).

4. Sensitivity to intrinsic variability: Upstream seeding

First, let us review the factors that determine the baroclinic eddy feedback in normal (non–El Niño) years to the quasi-stationary circulation (Orlanski 1998, 2003). Two key mechanisms complement each other to provide variability in the strength of the eastern ridge at the termination of the storm track:

1) The variability of the intensity and number of eddies from the Siberian storm track reaching the warm waters of the Pacific Ocean.
2) The relation of the intensity of the anticyclonic wave breaking with the poleward deflection of the storm track axis.

a. The seeding and downstream development

Since the early 1990s, a series of studies illustrated the importance of downstream development in the energy budget of baroclinic eddies in storm track environments (Orlanski and Katzfey 1991; Chang 1993; Orlanski and Chang 1993). The storm track shape and intensity depend on eddies decaying by fluxing energy downstream (Chang and Orlanski 1993, see review by Chang et al. 2002). Essentially we have baroclinic generation at the storm track entrance and barotropic decay at the exit. Downstream development extends the storm track from the more intense baroclinic source to the more depleted area in the middle of the storm track. Clearly, the storm track intensity may depend on the amount of wave activity entering the storm track. If there is a strong baroclinicity source, these waves will redevelop. For weak source instances (e.g., summer), waves will depend only on downstream development for growth and decay along the storm track. Eddies exiting Asia and entering the Pacific storm track exhibit considerable interannual variability. Based on 1983–99 data from the NCEP–NCAR reanalysis, a reasonable estimate could be as much as 50%.

Sensitivity experiments were performed with various seedings to understand, or at least determine, the eddy

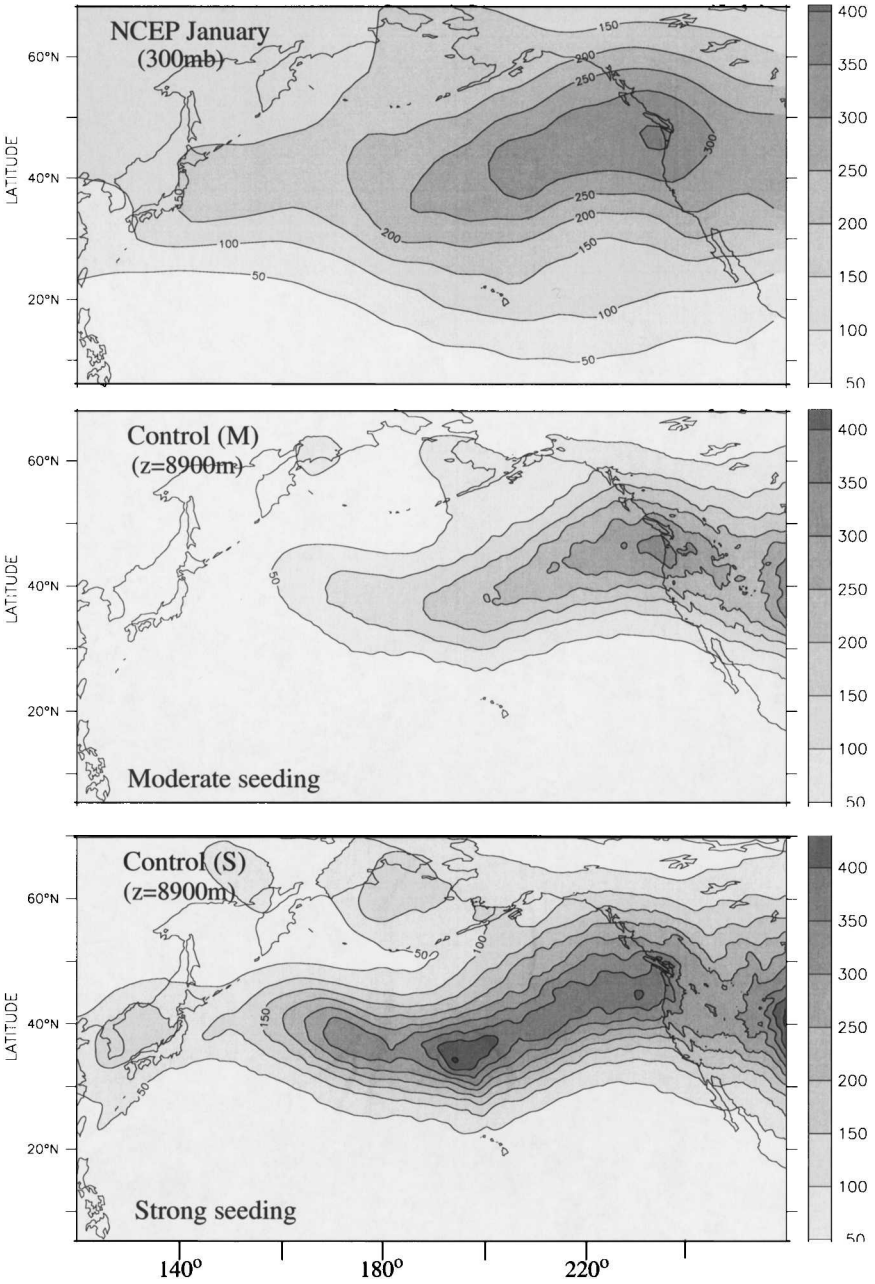

FIG. 4. Variance of the transient meridional velocity for the NCEP–NCAR reanalysis and two Control simulations. (top) Jan 300-mb variance of the meridional velocity from NCEP–NCAR reanalysis. The model simulations are at $z = 8900$ m, (middle) the "Control (M)" with moderate seeding, and (bottom) with strong seeding "Control (S)." The contour interval for all panels is 50 m^{-2} s^{-2}.

kinetic energy dependence along the storm track with respect to the amount of eddy seeding at the entrance. Figure 4 (middle panel) shows the eddy kinetic energy for moderate seeding, Control (M); the strong seeding, Control (S), is shown in the lower panel. The strong seeding tends to produce more intense mid storm track eddies. The time evolution of the seeding for two different meridional velocity amplitudes is shown in Fig. 5. Moderate seeding has a standard deviation of 4.08 m s^{-1} and the strong seeding is nearly double that, 7.93 m s^{-1}.

Baroclinic eddies in a storm track environment grow through baroclinicity and downstream development (Chang and Orlanski 1993). Therefore, eddies feel the influence of surface baroclinicity, which enhances their intensity and produces stronger energy fluxes down-

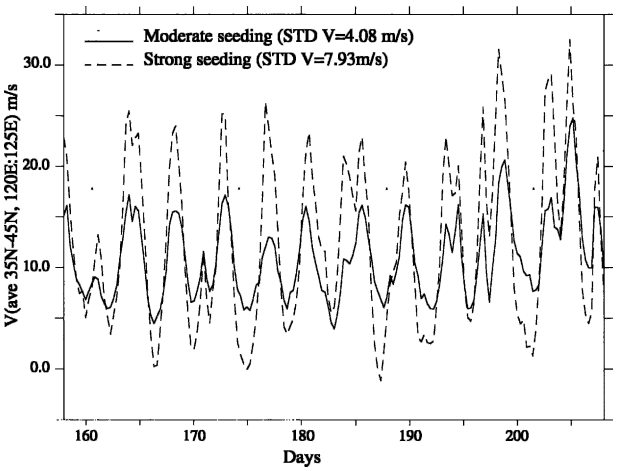

FIG. 5. The meridional velocity area average (10° × 10°) for Control (M) and Control (S), moderate and strong seeding, respectively. The seeding, although random in amplitude and frequency, is the same but the strong seeding has double the amplitude of the moderate seeding. Note that the plot shows the total meridional velocity, which is the velocity that the model produces by recirculation plus the nudged seeding.

stream to a new growing system. Consequently, strong baroclinic eddies in the western Pacific Ocean reach equilibration faster (near the storm track entrance) for more intense seeding. The initial amplitude is larger and the required zonal distance where eddies will mature is shorter. Figure 6 displays the Hovmoeller diagrams for pressure deviations of its time mean at z = 5500 m (around 500 mb) are shown for the Control (M) and Control (S) in the left and right panels, respectively. Let us highlight a few important features from these responses. First, the eddies clearly propagate downstream as seen in the anomaly field (left panel). The disturbances have synoptic time scales and there is a clear correlation pattern between large upstream disturbances and large downstream disturbances a few days later. Finally, the pressure difference (right panel) shows that the strong seeding produces a larger eddy response downstream. This raises some interesting questions.

- First, why is there an apparent strong asymmetry between highs and lows for the upstream disturbances?

The seeding meridional velocity, a sine function of time, is quite symmetric in Fig. 5; a mean meridional

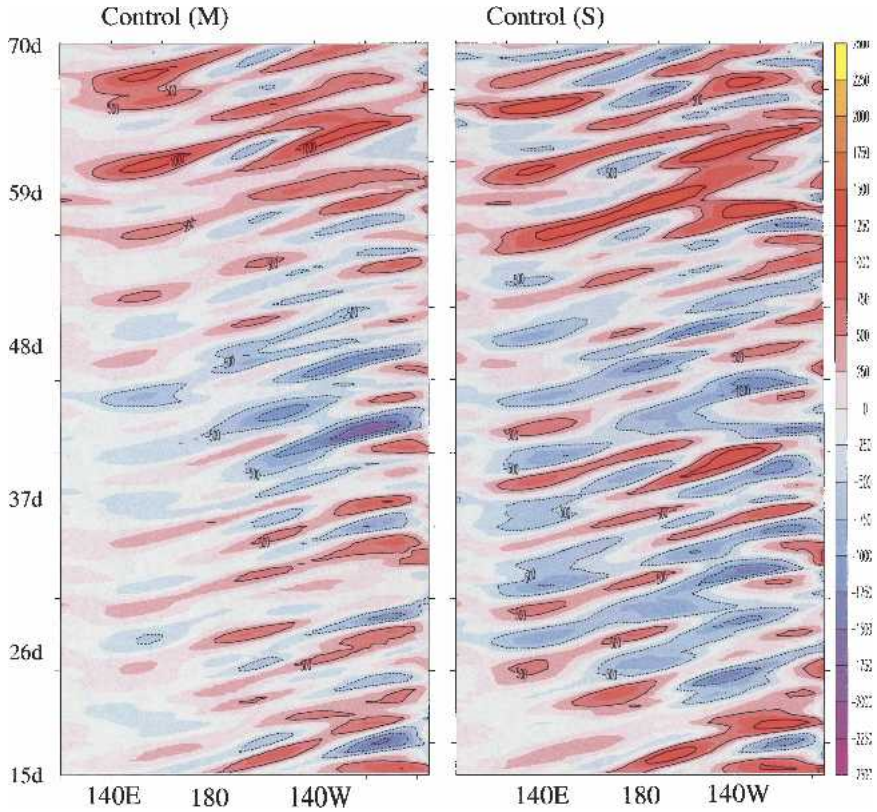

FIG. 6. Hovmoeller diagrams of pressure deviations: (left) Control (M) − Control (M) time mean and (right) Control (S) − Control (S) time mean. The contour interval for the panels is 4.0 hPa.

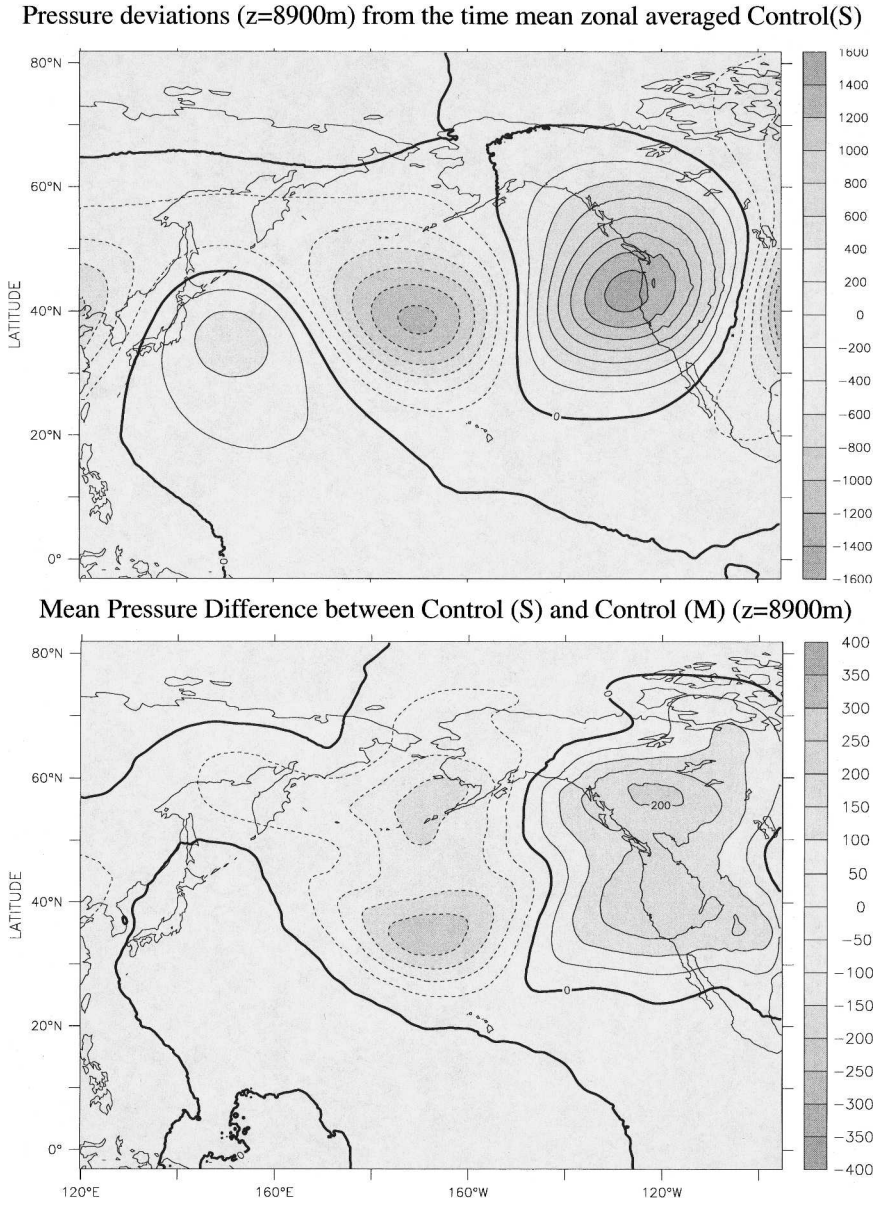

FIG. 7. The time-averaged (50 days) upper-level pressure for Control (S) (CI = 200 Pa, the maximum over the eastern Pacific is above 14 hPa) and the mean pressure differences between Control (S) and Control (M) (CI = 50 Pa).

circulation is also present. Note that, in non–El Niño (normal) years over the western Pacific Ocean a considerable amount of moist fluxes extend from the subtropics to the extratropics (lower-right panel in Fig. 3). As the poleward meridional flow becomes enhanced, more intense fluxes reach the baroclinic eddies (computed but not shown) and a more intense circulation is generates in comparison with the phase in which the meridional flow diminishes due to the equatorward phase of the seeding. This enhances the asymmetry between the anticyclonic and cyclonic circulation at the storm track entrance.

- Second, what relation exists between a stronger upstream high anomaly in the western Pacific and the response over the PNA sector?

Figure 6 suggests a clear signal of downstream development. This was confirmed by the meridional velocity time-lag regression from the meridional velocity time series at the storm track entrance (not shown here). The slope of the centers in this figure allows us to infer that the group velocity is about 40 m s^{-1} and the equal phase slope (phase velocity) is about 12 m s^{-1}. Both velocities closely correspond; specifically, the group ve-

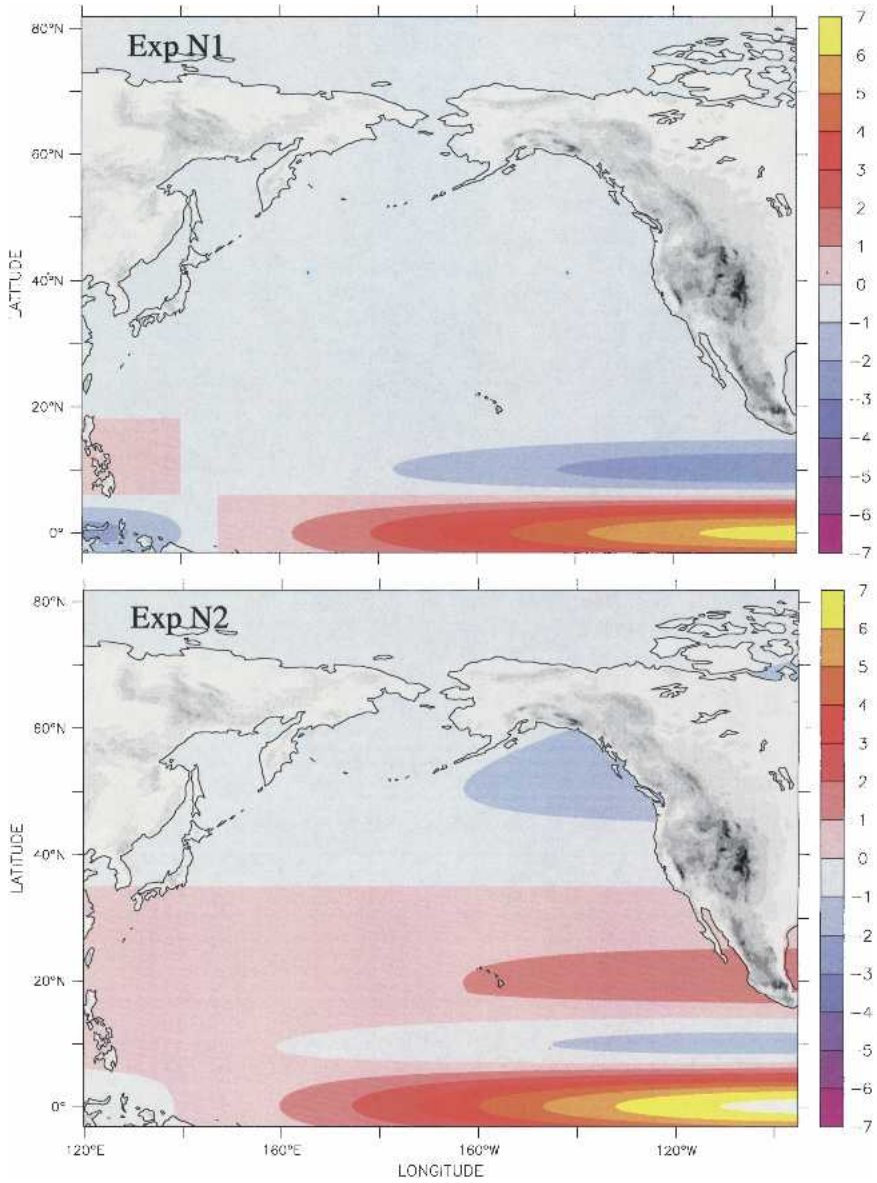

FIG. 8. SST anomaly from experiments (top) N1, moderate equatorial SST and (bottom) N2, strong equatorial SST. The contour interval is 1°C in both panels. (The maximum temperature anomaly in N1 is about 6°, and 7°C for N2.)

locity to the upper-level flow and the phase velocity to the steering velocity at around 4000 m; the velocity ratio is about $C_g/C_{ph} = 3.3$. The upper-level response due to the jet baroclinicity and speed has a zonal wavelength close to 56° longitude (4760 km, a global wavenumber m between 6 and 7) and does not seem to be very sensitive to small variations of the jet conditions. A simple geometric relation shows that with a velocity ratio of 3.3, a high center, H, located in the vicinity of the storm track entrance, (~140°E, pressure centers at $t = 0$,) will maximize the high response at a distance of roughly $3.3 \times \lambda/2$ from the initial high, or at around 130°W (140°E + $3.3 \times 56°/2$). Although not shown, results indicate that the larger the meridional flow is at the entrance, the larger its effect will be downstream. This result is crucial to understanding how intrinsic variability (here as high-frequency wave activity entering the storm track region) could drastically change the response in the PNA sector. Figure 7 (top panel) shows the upper-level mean pressure for the Control (S) (cf. to Fig. 3 upper-right panel) and the difference between the mean of Control (S) and Control (M) is shown in the bottom panel. Both panels show that Control (S) has a larger pressure height over the PNA sector.

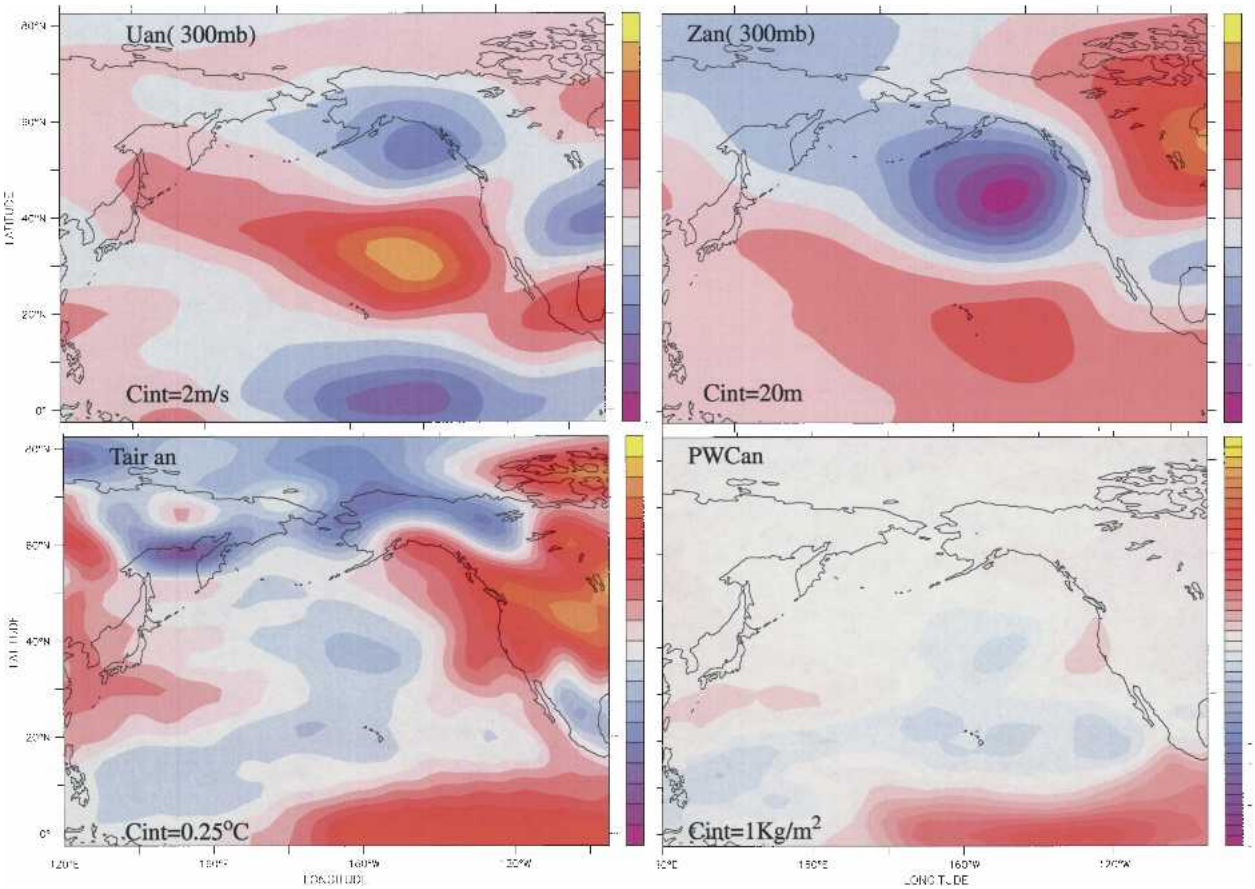

FIG. 9. The Jan CDC composite anomaly fields for El Niño years using Niño-3.4 time series (NCEP–NCAR reanalysis data). Variables are (top left) the 200-mb zonal wind anomaly (the shading key range is 14 and -14 m s^{-1}), and (top right) the 200-mb height anomaly (the shading key extrema are 140 and -140 m). (bottom left) Surface air temperature (shading key extrema are 2.5° and -2.5°C) and (bottom right) column precipitable water content (shading key extrema range from 20 to -20 kg m^{-2}). The zero contour is the boundary between the white and pink colors.

b. Upper-level wave breaking

As waves develop downstream they undergo a scale transformation. The eastern half of the storm track has less baroclinicity. Even if upstream fluxes cause the waves to grow larger, they become more upper-level barotropic with enhanced horizontal scales (Simmons and Hoskins 1979; Orlanski and Chang 1993). This scale expansion can be seen in the time mean upper-level pressure anomalies in Fig. 3 (upper-right panel), and there are hints of scale expansion in the midlevel pressure disturbances in the Hovmoeller diagram in Fig. 6. For moderate and strong seeding, upper-level waves will complete their life cycle and break as they propagate eastward. The more intense the baroclinic waves are, the more intense the wave breaking is and, as shown by Orlanski (2003), the axis of the storm track will be deflected farther poleward, thus enhancing the *ridge* over the PNA sector. Orlanski (2003) also shows that, if the eddy energy is very intense, a bifurcation in the life cycle can occur. Then, instead of waves breaking anticyclonically, they could break cyclonically pushing the axis and the jet more equatorward. The energy level at which the shift is possible is strongly dependent on the horizontal scale of the waves. There is currently no reliable statistical measure of counting the number of waves that break one way or another. A superficial estimate of the energy level for the control solution shows that the level is insufficient for bifurcation to occur for these wavelengths. Orlanski (2003) estimates (his Fig. 18) that a wavenumber $m = 7$ should reach at least 400 (m s^{-1})^2 and for $m = 6$ more than 500 (m s^{-1})^2 for bifurcation to occur. Both solutions (moderate and strong seeding) fall short of these threshold energies.

Before concluding this section we should clarify the role of seeding in the PNA sector. We already know the effects of intense seeding, but a valid question is: *what happens if no seeding or a very small seeding is introduced in the western Pacific?* A simulation with a very small seeding was done (0.1 the moderate seeding amplitude). The results are very similar to the moderate seeding. Remember that with or without seeding, the

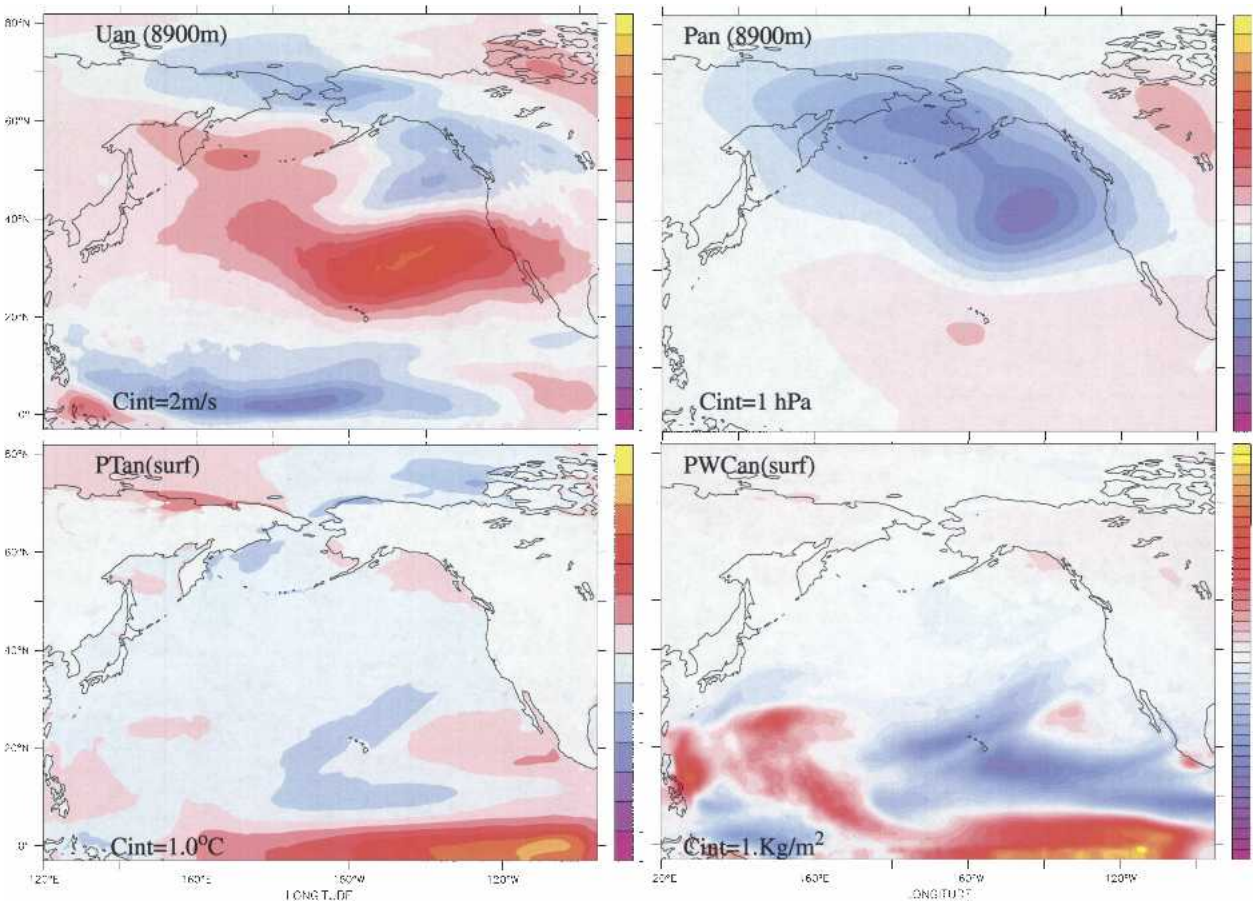

FIG. 10. Analogous to Fig. 9 but for the simulations. The anomaly fields between N1 and Control: (upper left) the zonal wind at 8900 m (the shading key extrema are 14 and -14 m s^{-1}), (upper right) the pressure anomaly at $z = 8900$ m (the shading key extrema are 11 and -11 hPa), (lower left) the surface potential temperature anomaly (the shading key extrema are 7° and -7°C), and (lower right) the precipitable water content (the shading key extrema are 20 and -20 kg m^{-2}). The zero contour is the boundary between the white and pink regions.

entrance of the storm track is baroclinically unstable. However, it is of the convective instability kind rather than the absolute instability (Pierrehumbert 1984). It means that for a permanent response it should have a constant seeding. The initial disturbance produced by the seeding helps increase the eddy development to a finite amplitude closer to the entrance region. Regardless of the imposed seeding level at the entrance, there is a constant background seeding from perturbations that recycle from the western subtropical convective region as well as disturbances entering from the western high latitudes to the storm track region. Since our so-called open boundary conditions (Orlanski 1976; Haltiner and Williams 1979) are not perfect, some disturbances that propagate westward, whether in the Tropics or high latitudes, may be forced to recycle. This is why baroclinic eddies are not as dependent on the shape and frequency of the seeding as they are on the amplitude exceeding a critical level (approximately the value used for our moderate seeding). Now that we have a better understanding of the response to normal SST conditions and the variability to external seeding, we can analyze the conditions for tropical SST anomalies.

5. Sensitivity to tropical SSTs

a. Mean anomaly conditions due to changes in tropical SST

Using a format similar to section 4, we introduce a temperature anomaly to the SST shown in Fig. 2. This is the control experiment [for convention, the control experiment used hereafter is the moderate seeding case Control (M) previously discussed]. For comparison, two El Niño experiments with modified SSTs, N1 (moderate) and N2 (strong) are presented. Their SST anomalies from Control (M) are shown in Fig. 8. We see enhanced temperatures in the eastern ocean confined to the tropical region.

Experiment N2 has a maximum anomaly of 7°C (note the larger temperature anomaly area). Since our

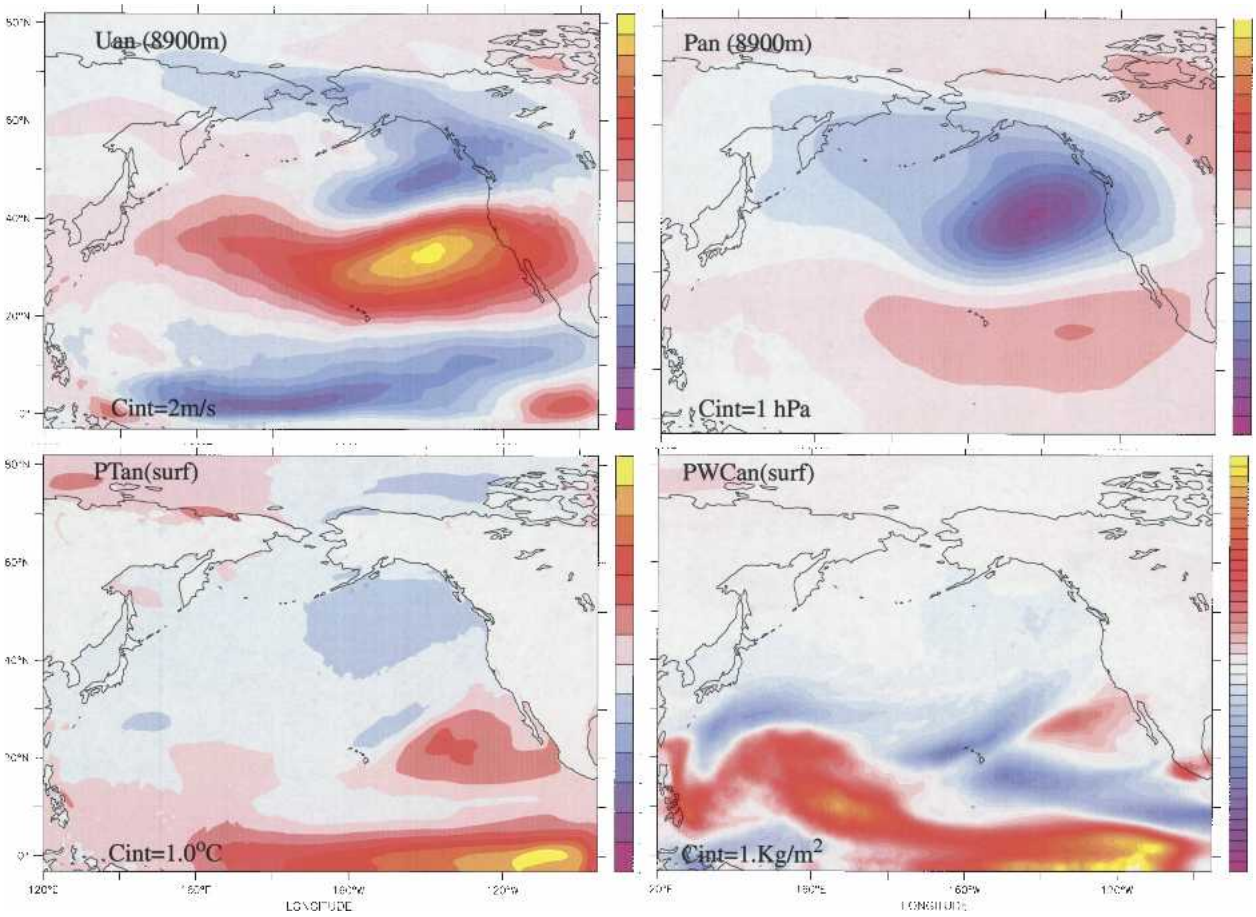

FIG. 11. Similar to Fig. 10 but for the anomaly fields between N2 and Control: (upper left) the zonal wind at 8900 m (shading key extrema are 14 and -14 m s^{-1}), (upper right) the pressure anomaly at $z = 8900$ m (shading key extrema are 11 and -11 hPa), (lower left) the surface potential temperature anomaly (shading key extrema are 7° and -7°C), and (lower right) the precipitable water content (shading key extrema are 20 and -20 kg m^{-2}). The zero contour is the boundary between the white and pink regions.

approach has been to determine the level of high-frequency eddy activity and its feedback to the quasi-permanent flow, it is important to show that not only the so-called PNA can be reproduced but also the anomaly amplitudes as well. For that purpose we show the observed anomalies from the NCEP–NCAR reanalysis as provided by the National Oceanic and Atmospheric Administration–Cooperative Institute for Research in Environmental Science (NOAA–CIRES) Climate Diagnostics Center (CDC; data available online at www.cdc.noaa.gov) in Fig. 9. The anomalies shown are January of El Niño years for the period 1958–2004 minus climatology (1968–96). The 300-mb mean zonal wind deviations (upper left panel) indicate an equatorward deviation of the jet. The characteristic PNA pattern appears in the 300-mb height analysis (upper right panel). Surface air temperature and precipitable water column are displayed in the lower panels (left and right, respectively). Consistent with the equatorial temperature shift to the east, the precipitable water also has been displaced to the east.

Figures 10 and 11 are fashioned similar to Fig. 9 for comparison. However, pressure anomalies and surface potential temperature anomalies are shown at heights compatible with the fields in Fig. 9. The simulations, N1 and N2, exhibit a rather similar pattern; however, both are shown to illustrate intensity differences. Experiment N2, characterized by a stronger SST but the same seeding as N1, has anomalies all larger than N1. Although the fields are different, similarity patterns with the observed anomalies (Fig. 9) are easily recognized. The zonal flow, with the same scale (2 m s^{-1}), also shows a very similar displacement to the Tropics. The PNA pattern again has strong similarities; the minimum pressure anomaly in the simulation is about 8 hPa or about 184 m (at 300 hPa, 23 m hPA^{-1}) for N2 (Fig. 11), whereas for N1, it is 6 hPA (Fig. 10) and the observed anomaly is about 120 m in Fig. 9. Although it is more difficult to make a direct quantitative comparison with the other two fields, the overall patterns seem quite satisfactory. This is particularly noticeable for the negative precipitable water in the west-

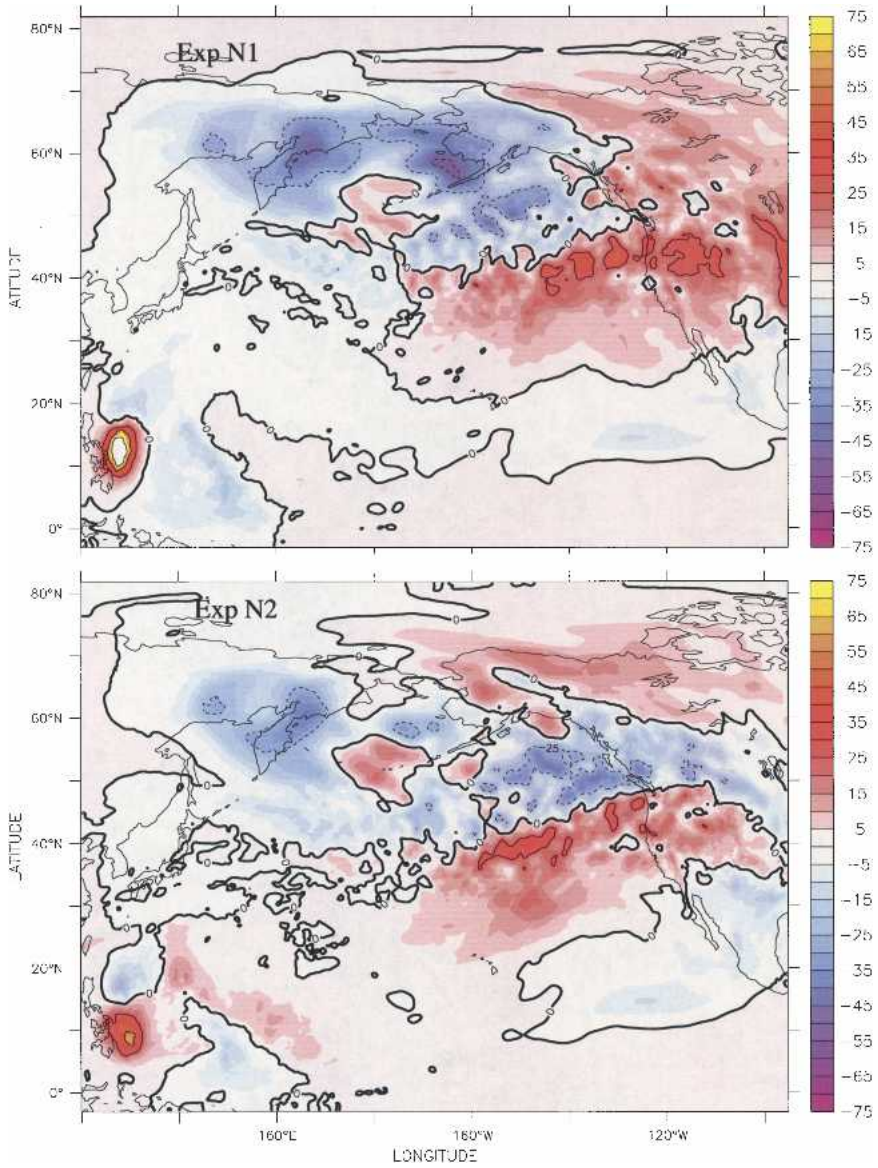

FIG. 12. The anomaly eddy kinetic energy ($z = 5500$ m) is shown for both El Niño experiments: (top) N1 − Control and (bottom) N2 − Control (the shading interval is 5 m^{-2} s^{-2}).

ern Tropics and the strong positive anomaly east of the date line. However, the simulations show a stronger precipitable water anomaly in the western subtropics not shown in the observations. This may be the result of the unrealistic warm pool in the western subtropics for the idealized SST used.

b. Anomalies in wave activity

The eddy kinetic energy anomalies for N1 and N2 are shown in Fig. 12. Both show a distinct equatorward displacement of the storm track. The anomalies in both experiments appear very similar and have amplitudes equal to 15%–20% of the total eddy kinetic energy. Values for N1 seem larger than N2, and this issue will be discussed later. The western subtropic anomaly shown in Fig. 12 is a product of a minimal but persistent convective activity for the ENSO warm phase simulations. Although this may be an artifact of the idealized SST and western boundary condition used in the simulations, these disturbances did not seem to affect or interact with the storm track. The effect of tropical SSTs on the extratropical pressure disturbance can be seen in Fig. 13 (similar to Fig. 6). The Hovmoeller diagram shows, in this case, the pressure deviation from the time mean Control (M), N1, and N2. (Note that the meridional extent of the averaging is sufficiently large to encompass any meridional displacement expected

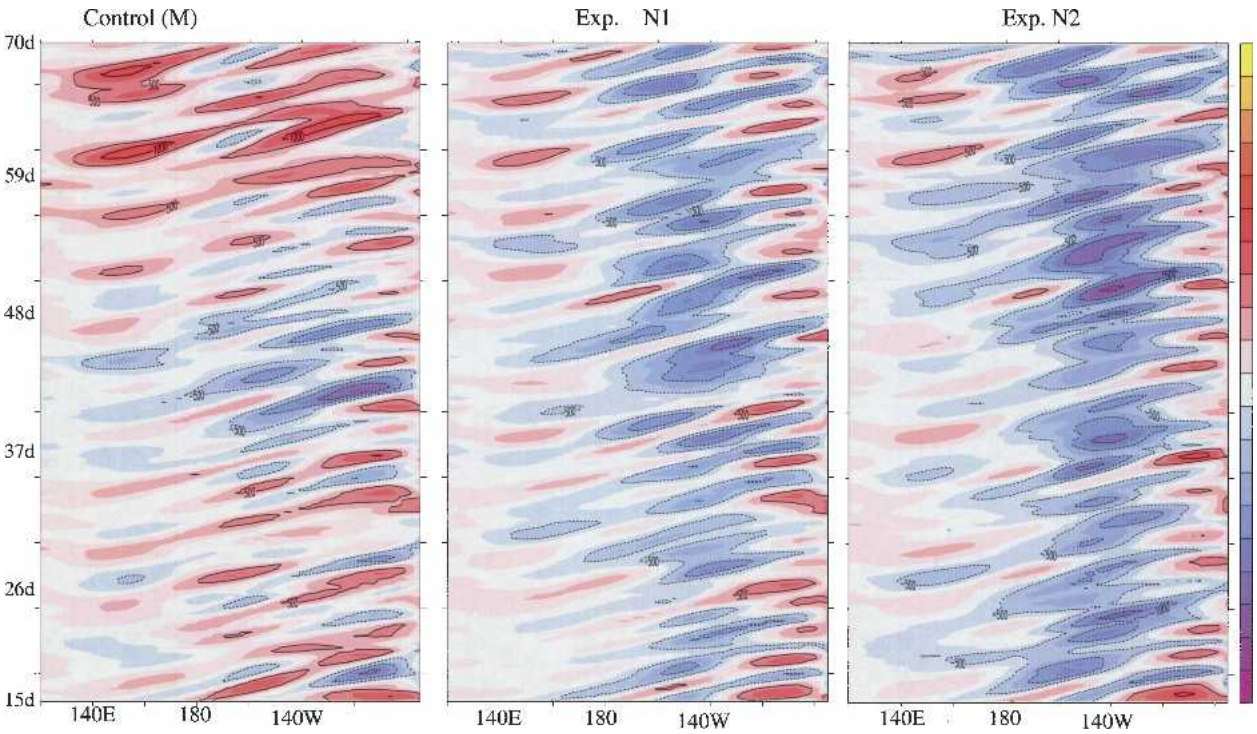

FIG. 13. Hovmoeller diagrams: (left) Pressure deviation for Control, (middle) N1, and (right) N2; the deviations are from the time mean conditions of Control (M) (similar to Fig. 6). Again, blue indicates low pressure and red high pressure (CI = 2.5 hPa, shading key extrema are 25 and −25 hPa).

for the storm track.) Since the seeding is the same in all three cases, we present the Hovmoeller diagram for pressure difference from the Control time mean to enhance the view that high frequencies tend to reinforce the pressure anomalies (e.g., in Fig. 18, the pressure disturbance of N1 is shown as a deviation of its time mean). In all cases two distinct differences in the pressure response are immediately apparent. Although the seeding amplitude is the same, Control has a slightly larger amplitude at the storm track entrance and a much larger amplitude at the exit. On the other hand, N2 with the stronger tropical SST has the weakest amplitude. Furthermore, the trough in the middle storm track seems consistently more intense for the stronger El Niño case (N2). It seems evident that high-frequency eddies have a considerable influence on the enhancement or weakness of the quasi-permanent disturbance in the eastern Pacific Ocean. Clearly, downstream development from the western ocean is present in most cases with varying degrees of intensity. Additionally, N1 and N2 having approximately the same intensities in the western Pacific Ocean, the stronger SST anomaly case shows a consistently weaker intensity of the ridge over the PNA sector. Consequently, we may conclude that baroclinic eddies are probably primarily responsible for storm track sensitivity to tropical SSTs. We will investigate how sources and sinks for those eddies can change due to changes in the tropical circulation.

c. *Sources and sinks*

Analysis of the heat flux anomaly in the lower layers of the atmosphere suggest that both N1 and N2 have more poleward heat fluxes than Control on the equator side of the storm track (not shown here). This suggests that more baroclinicity should be extended equatorward for the El Niño cases. A number of studies have examined the eddy energy budgets of baroclinic waves (e.g., Smith 1969; Kung 1977; Orlanski and Katzfey 1991; among others). Employing the form and interpretation of the budget suggested by Orlanski and Katzfey (1991) yields a budget of the form

$$\frac{\partial E}{\partial t} = -\nabla \cdot \overline{\langle \mathbf{v}E + \mathbf{v}_d' p' \rangle} - \frac{g(\overline{\mathbf{v}'\theta'} \cdot \nabla\Theta)}{\Theta_m \left\langle \frac{\partial \Theta}{\partial z} \right\rangle} - \overline{\mathbf{v}' \cdot \langle \mathbf{v}' \cdot \nabla \rangle V_m} - \text{diss} + \text{diab},$$

where the bar indicates the time average for the period, the prime indicates the deviation of that average, and angle brackets indicate a large area and time average. The first term on the rhs is the energy and pressure fluxes, the second term is the baroclinic conversion, the

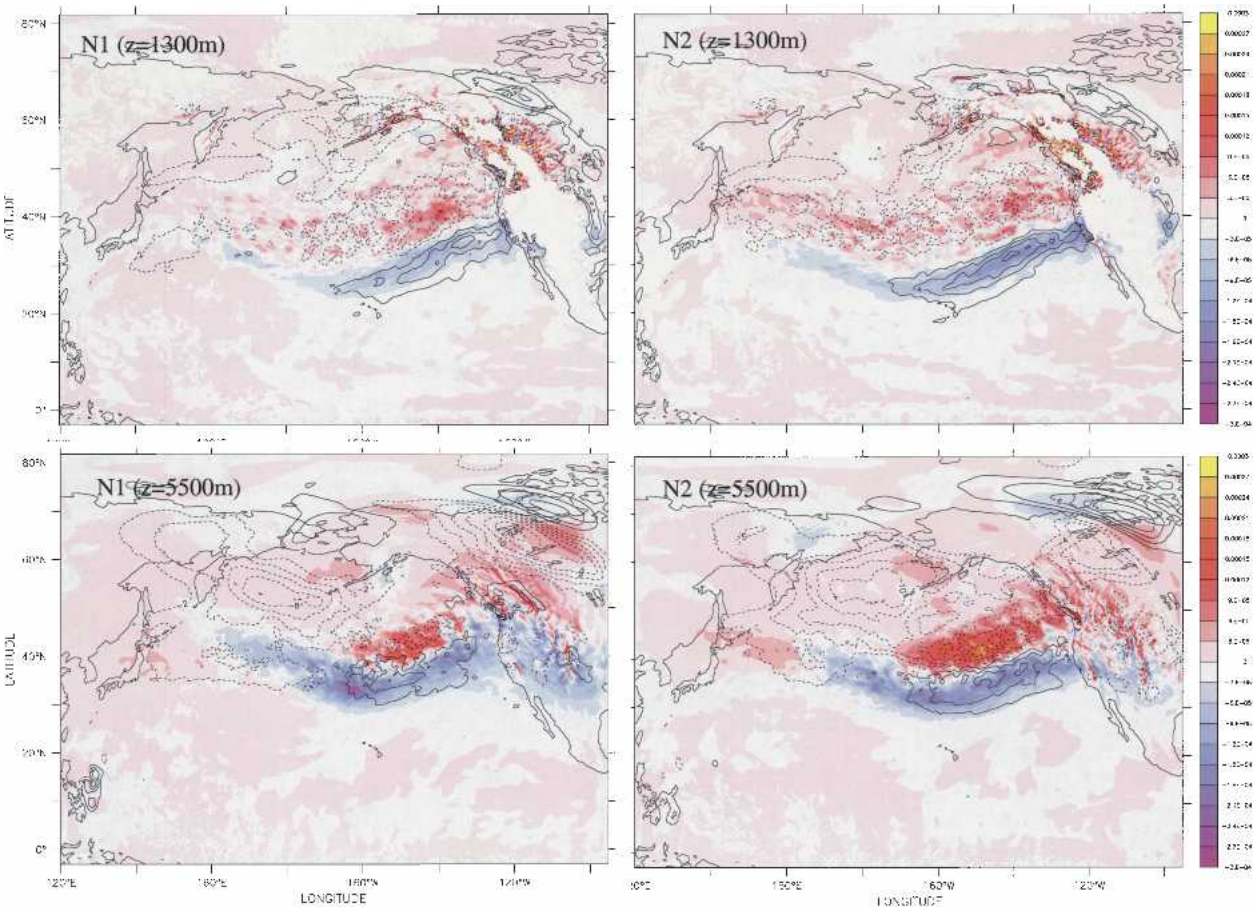

FIG. 14. Baroclinic conversion anomalies and potential temperature variance for N1 and N2 shown at (upper left and upper right) 1300 and (lower left and lower right) 5500 m. Positive eddy energy anomalies are shaded blue.

third term is the barotropic conversion and the last two terms are the dissipation and diabatic effects. Note that the convention used for baroclinic and barotropic conversion has a positive tendency for the eddy energy when either one is negative.

The baroclinic conversion anomaly for N1 and N2 is shown in Fig. 14 for two levels $z = 1300$ m and $z = 5500$ m. For N1 and N2 the salient characteristic is more baroclinic conversion on the equator side of the eastern storm track. Contours show the variance of the eddy potential temperature anomaly, which is consistent with the eddy kinetic energy anomaly (Fig. 12). Both experiments have larger values on the southern side. Figure 14 allows us to conclude that baroclinic conversion is being displaced equatorward. Upper-level barotropic conversion was also analyzed and, although not shown, exhibits the same features. Control has a more intense barotropic conversion on the poleward side than either El Niño experiment. To summarize, both N1 and N2 have an intensified baroclinic generation over the mid-Pacific region and stronger pressure fluxes over the southeastern ocean and the west coast of North America. Both N1 and N2 appear to have a more intense source of baroclinicity over the subtropical eastern part of the Pacific Ocean.

d. Baroclinic sources

Figure 15 shows the potential temperature anomaly for El Niño years from the NCEP–NCAR reanalysis at 500 mb in the upper panel; the lower panel displays the potential temperature anomaly for N2 at $z = 5500$ m (N1, having a very similar pattern, is not shown). This level was selected because, as Fig. 14 showed, the baroclinic conversion extends deep into the atmosphere. Despite the quantitative differences, there is a remarkable qualitative similarity between the idealized simulations and the observed anomalies. Both the observed and simulated cases have increased baroclinicity around 30°N, a region associated with the maximum divergence of heat fluxes. Simulations seem to indicate that the warm region is related to the equatorial convective region and SST anomalies are being displaced eastward.

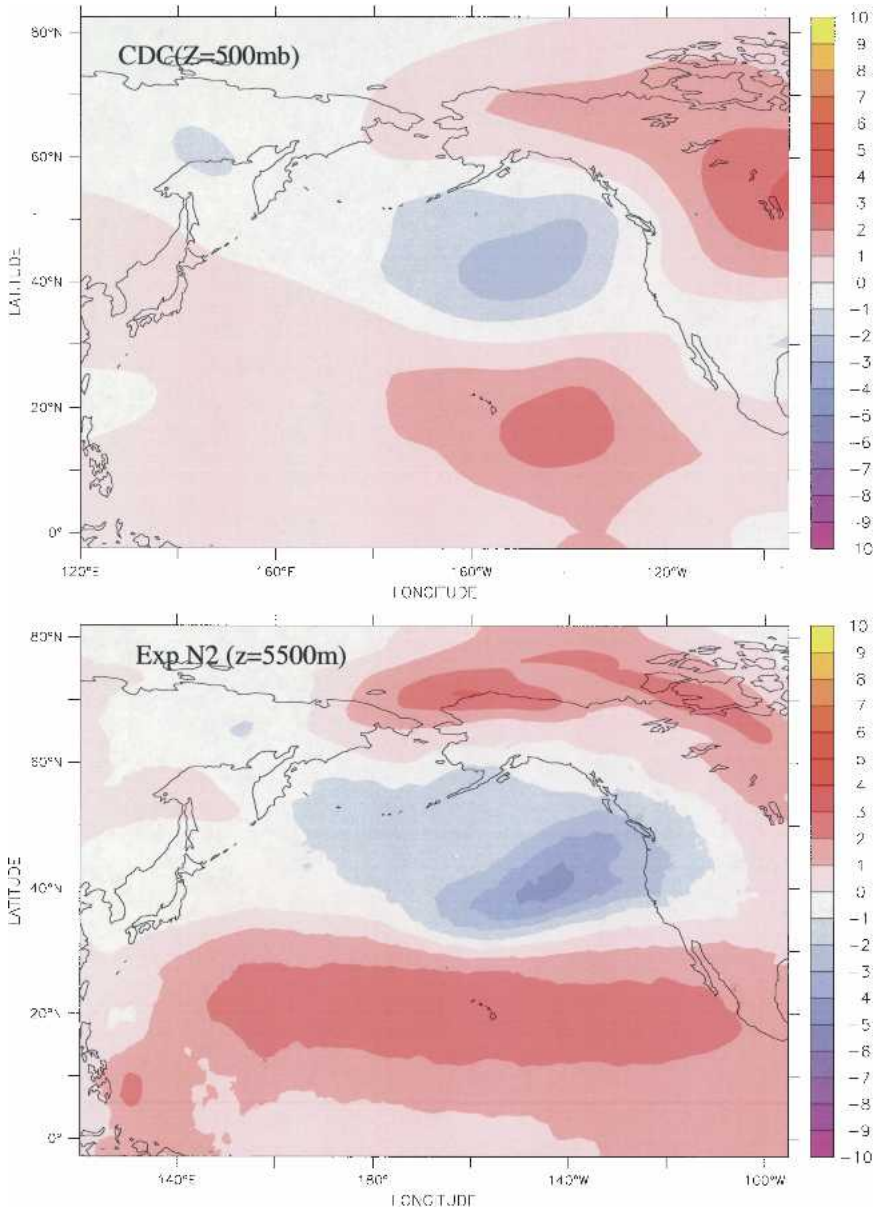

FIG. 15. Time mean potential temperature anomalies: (top) Jan of El Niño years from the NCEP–NCAR reanalysis (CDC) at $z = 500$ mb and (bottom) N2 − Control (M) at $z = 5500$ m. The shading interval is 1°C.

A zonally averaged (from 180° to 140°W) cross section of the potential temperature, liquid water, and meridional wind vector anomalies are shown in Fig. 16 for N2. There is a large temperature anomaly over the entire subtropical region with a very deep baroclinic zone in the middle latitudes, which is consistent with the previous figure. The warm anomalies seem very well correlated with the liquid water anomaly (proxy for latent heat) and also are consistent with the poleward meridional circulation of the Hadley circulation. The cold anomaly in the upper tropical and subtropical atmosphere is related to the lifting of the tropopause due to more intense convection. The reanalysis displays a similar pattern (not shown here).

e. SST forcing and intrinsic variability (upstream seeding)

1) TYPE OF WAVE BREAKING

The conclusions for wave seeding effects in the western Pacific Ocean (section 4) clearly show that the stronger the waves are entering the storm track, the sooner they reach equilibration amplitude and, due to downstream development, the more intense the upper-

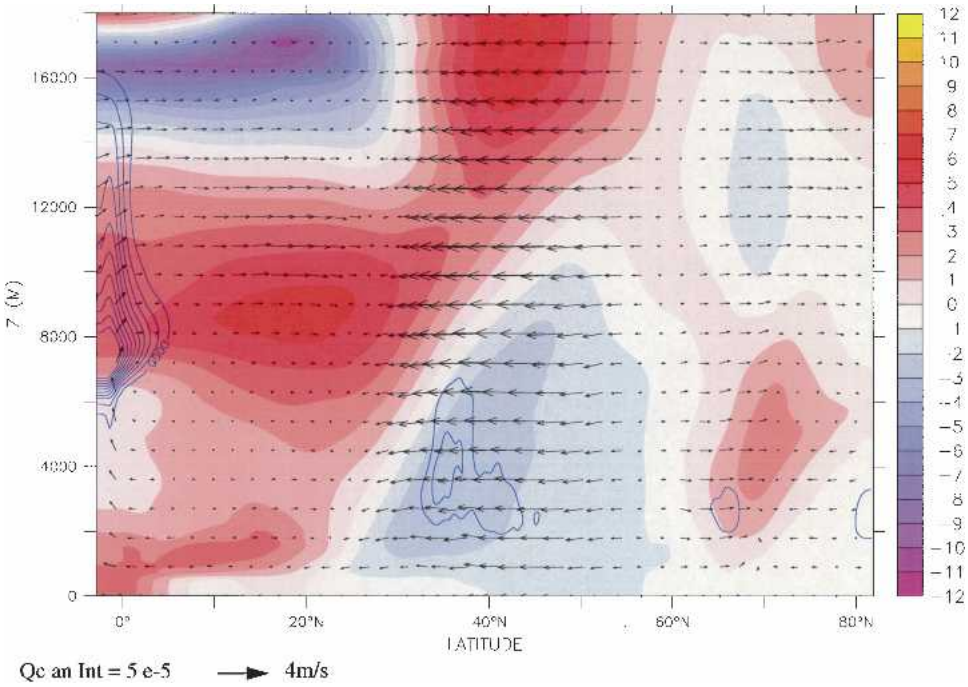

FIG. 16. Time-averaged potential temperature anomaly cross section for N2 − Control (M) (color shading), Qc, the liquid water content anomaly (blue contours), and meridional vector anomalies (vertical velocities are multiplied by a factor = 50). These fields are averaged over 40° longitude and centered at 160°W.

level disturbances are that reach the eastern Pacific coast. On the other hand, eastward movement of equatorial SSTs (El Niño conditions) produces a more intense baroclinic zone in the middle of the Pacific storm track. Consequently, stronger cyclonic developments occur south of the climatological (Control) storm track. Cyclonic development due to enhanced baroclinicity in the eastern storm track seems to compete with eddies entering from eastern Asia reducing the amplitude of the ridge over the PNA sector. Both mechanisms exhibit a different scale selectivity. Baroclinic eddies that develop from eastern Asia seeding feed on the baroclinicity at the storm track entrance. Since low-level baroclinicity for these cases is rather weak in the middle to eastern Pacific basin, downstream development causes a tendency for them to expand on the zonal scale and become more barotropic. Baroclinic waves flux energy downstream predominantly in the upper levels. Since they do not have a strong low-level source, they become upper-level barotropic waves with expanded zonal scales. To the contrary, for cases in which SST anomalies are to the east (El Niño years), subtropical baroclinicity in the middle to eastern Pacific Ocean enhances considerably and eddies that develop or redevelop there remain with a shorter scale more characteristic of cyclone waves. A regression analysis on the pressure anomaly for extreme experiments: the Control (S) (strong seeding), previously discussed, and the strong SST anomaly case (N2) suggests that

1) the size of the time mean pressure deviations in the PNA sector have roughly the same size as the regressed transient waves and
2) the zonal scales of the disturbances are considerably different for the Control (S) (~2955 km, global wavenumber m ~6.8) and the SST (N2) (~2333 km, m ~8.6) simulations.

From 1) and 2) we reach two major conclusions: the time mean anomalies are being produced by transient eddy feedback and western Pacific sources produce longer waves over the eastern Pacific that could break anticyclonically. Whereas, for cases where the baroclinicity source is moved to midocean (N2), resulting waves could experience cyclonic wave breaking.

Since the experiments have a short time span, 70 days, we cannot filter the disturbances with high-pass and low-pass frequencies and the result may seem questionable. As a means to corroborate these suggestions, arbitrary snapshots of the upper-level pressure and winds for Control (M) and N2 over four consecutive days are shown in Figs. 17a and 17b, respectively. Control (M) tends to produce large ridges over the eastern sector with hints of anticyclonic breaking. A rather different picture can be seen in Fig. 17b for N2 where there is a tendency for less ridge building and more cyclonic breaking. These results are reminiscent of those reported by Shapiro et al. (2001) for a rather limited analysis period (1997–99) over the PNA sector.

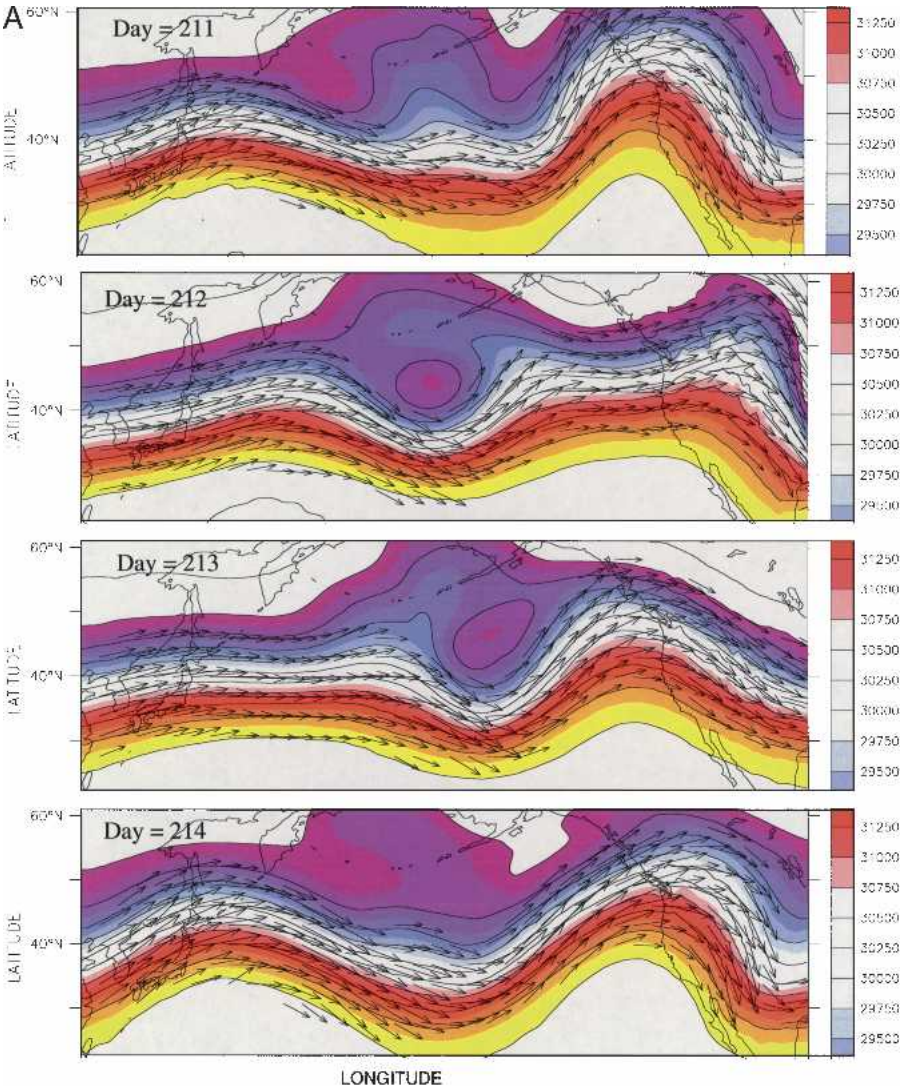

FIG. 17a. Snapshots of four consecutive days of upper-level pressure (color shading) and wind vectors for Control (M); for clarity only a reduced latitudinal band is shown (20°–60°N). Note the ridging in the eastern Pacific shows a clear anticyclonic wave breaking signature.

They estimated that more than 20 cyclonic wave breaking events occurred over the PNA sector in an El Niño year and only a few anticyclonic wave breaking events in the same year. However, they found the opposite for the following year, a negative phase of the ENSO cycle.

2) RESPONSE TO SST ANOMALY FOR MODERATE AND STRONG UPSTREAM SEEDING

The two competing mechanisms, western upstream seeding and the central ocean baroclinic anomaly, give a strong variability to the response of the ENSO cycle. To prove this conjecture, we ran a simulation with N1 SST conditions but added the strong seeding as described for the Control case in section 4 (see Fig. 5). Figure 18 shows the Hovmoeller diagrams of pressure deviations of the Control (M) (moderate seeding), N1 [moderate seeding, hereafter N1(M)] and the new simulation N1 [strong seeding, hereafter N1(S)] in the left, middle, and right panels, respectively. Figure 18 is very similar to Fig. 13, but here the anomalies are with respect to each time mean rather than from the Control (M) mean. The solutions are qualitatively quite similar. Clearly the pressure height anomaly in the western Pacific for N1(S) seems stronger than either the Control(M) or N1(M). As a consequence of the stronger seeding, the height over the eastern PNA sector for N1(S) is also stronger than N1(M). The pressure anomaly for N1(M) (top panel) and N1(S) (bottom panel) at $z = 8900$ m shown in Fig. 19 corroborate this result. Although there is a qualitative resemblance between both responses, obviously the strong seeding has

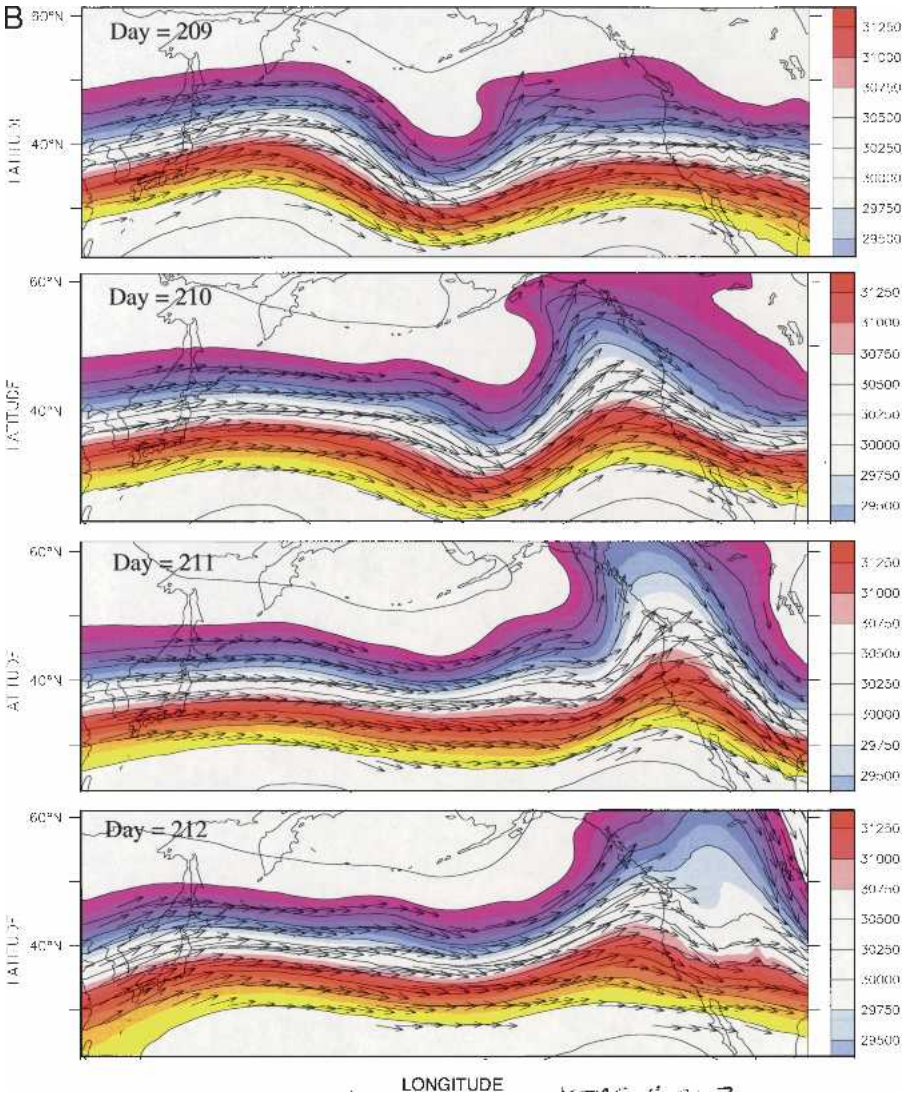

FIG. 17b. As in Fig. 17a but for N2. This figure shows a cyclonic wave breaking tendency.

weakened the anomaly considerably (about 70%). The SST anomaly pushes the subtropical jet, baroclinicity, and storm track equatorward whereas the stronger seeding at the storm track entrance due to the downstream development produces upper-level barotropic waves in the eastern Pacific with predominantly anticyclonic wave breaking and poleward momentum fluxes.

6. Summary and conclusions

The work presented is quite distinct from the many articles written on the subject. First, a high-resolution nonhydrostatic cloud resolving model is used to simulate the Pacific storm track and its sensitivity to tropical SST intrinsic variability (upstream seeding). The experiments are designed to treat upstream seeding and the effect of tropical SST anomalies independently. This study has three goals to assess:

- How much the intrinsic variability, measured as high frequency waves entering the western Pacific storm track, canaffect the response over the eastern sector.
- How tropical anomalous SSTs can produce the well known response over the PNA region.
- How intrinsic variability interferes with the surface boundary forcing to provide a great variability in the storm track response on the PNA region.

The study first considers the "normal" (non–El Niño) years. Storm track seeding effects by waves entering from the Asian continent are investigated. Two mechanisms operate to distribute the eddy energy along the storm track: downstream development and baroclinic

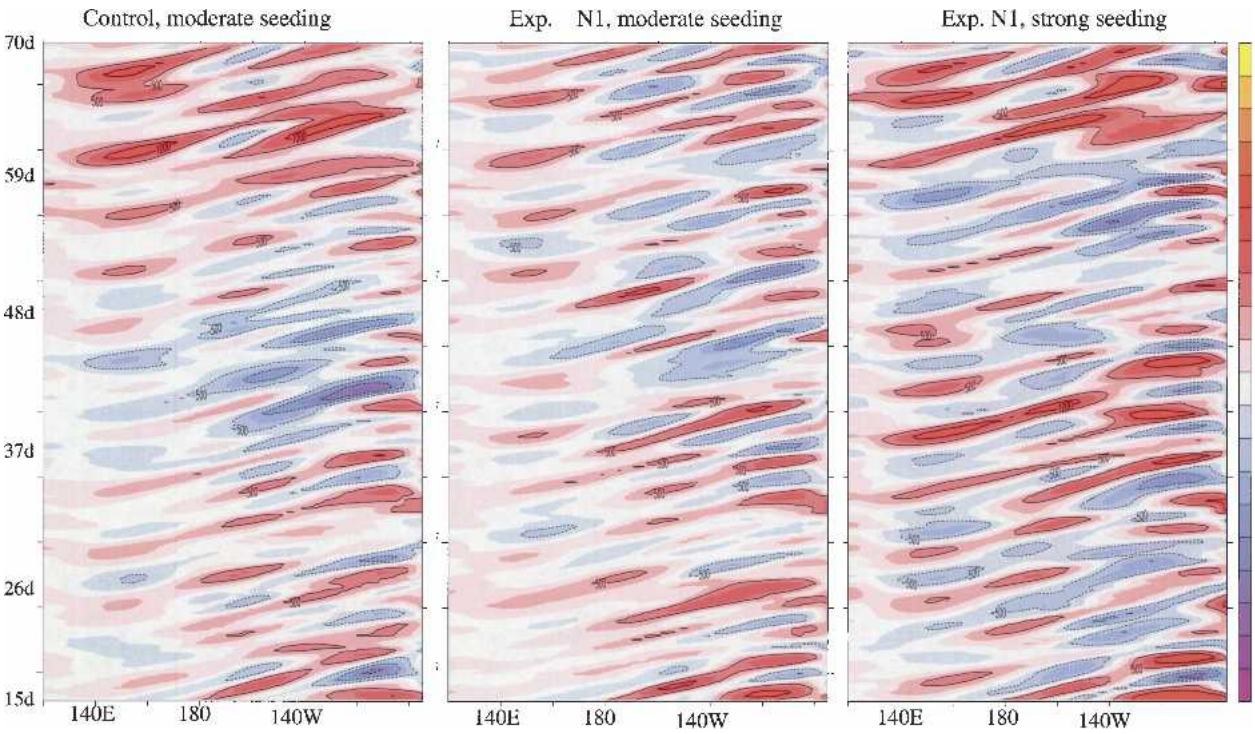

FIG. 18. Hovmoeller diagrams of pressure deviation from the corresponding time mean for (left) Control (M) (moderate seeding), (middle) N1(M) (moderate seeding), and (right) N1(S) (strong seeding). Again, blue indicates low pressure and red high pressure (CI = 2.5 hPa, shading key extrema are 25 and −25 hPa).

development. The large effect on baroclinic development at the storm track entrance results from a combination of factors: surface baroclinicity, land–sea contrast, and strong moist fluxes from the western subtropics. The large longitudinal baroclinicity gradients, a maximum at the storm track entrance, are attributable to large temperature and moisture flux gradients from land to ocean and baroclinicity variability over the ocean. As eddies grow from the entrance and along the storm track, they mix the ocean SST and thus reduce the baroclinicity along it. Moreover, waves entering the storm track from the cold continent receive a considerable amount of surface heat fluxes that energizes them. Large amounts of moisture in the western subtropics during non–El Niño years is an extra source for wave growth. This explains why the seeding amplitude sensitivity in our experiments, Control (M) versus Control (S), is so large. The larger the seeding amplitude is, the closer the more intense baroclinic waves and intense wave breaking are to the entrance. This is consistent with Orlanski (2003); the axis of the storm track will be deflected farther poleward, thus further enhancing the *ridge* over the PNA sector.

Sensitivity to SST anomalies shows qualitative and quantitative similarity with observed anomalies. Upper-level zonal wind pressure patterns and eddy kinetic energy show a very similar displacement toward the Tropics. Tropical surface air temperatures and column liquid water are displaced eastward during observed ENSO warm phases. Experiments show that the PNA pattern is enhanced for a stronger SST anomaly (N2 with respect to N1). Those cases also identify the existence of a secondary source of baroclinic development in the middle of the storm track (date line), which was also shown by Orlanski (1998) for a small number of observed ENSO cycles. Further investigation relates the increased baroclinicity in the mid-Pacific to the fact that stronger convection in the midtropical Pacific enhances a large pool of warm air over the entire mideastern subtropical ocean. This warm air pool is the enhanced baroclinicity source in the region. Eastward displacement of the baroclinic zone in El Niño years produces an extra source for baroclinic development in the mideastern Pacific Ocean. The resulting baroclinic waves tend to reduce the effects over the PNA region of waves originating at the storm track entrance; however, these waves break anticyclonically and produce the eastern Pacific ridge. The baroclinic waves generated or regenerated in the middle of the ocean tend to break cyclonically and produce a trough tendency, by then reducing the amplitude of the eastern ridge.

Two main effects play an important role in maintaining the quasi-permanent circulation: downstream development from the storm track entrance and the displaced baroclinicity in the mid-Pacific for El Niño conditions. Experiment N1(S), a simulation with strong

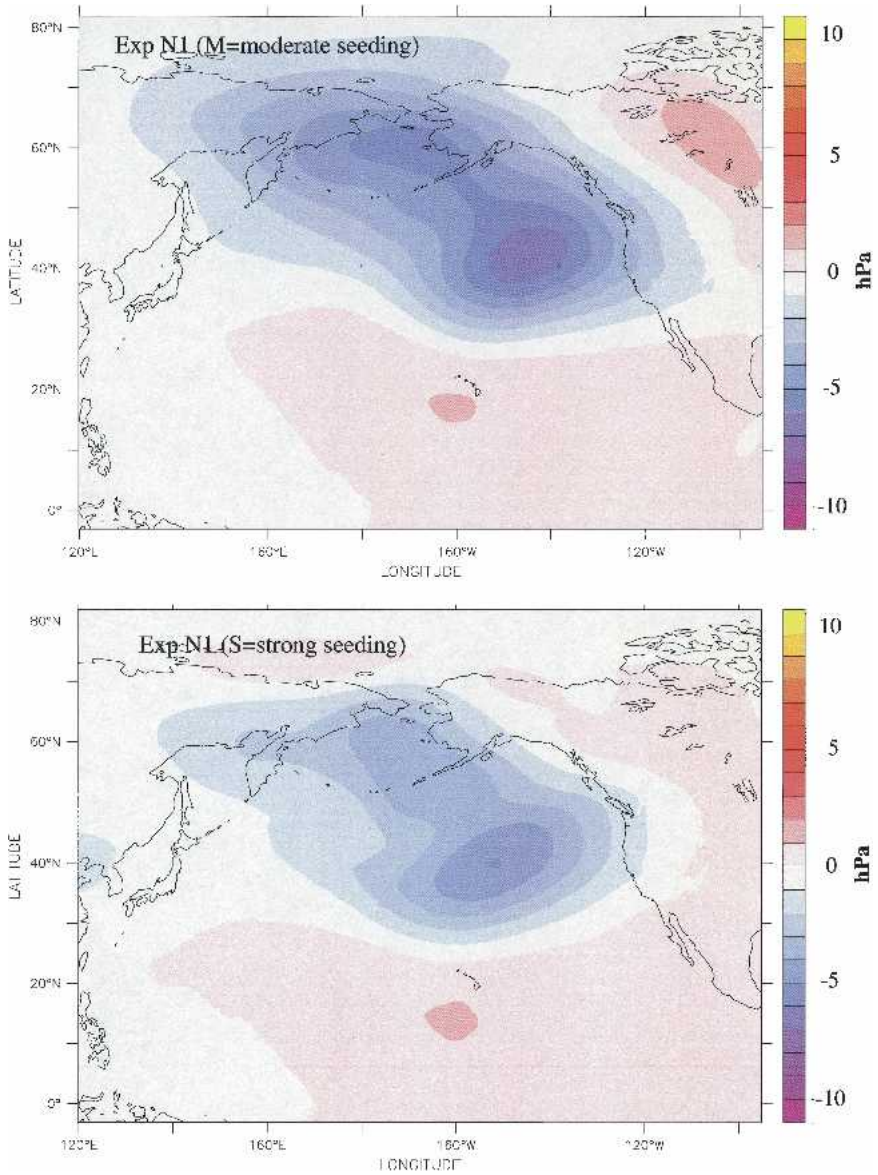

FIG. 19. Upper-level pressure anomaly for (top) N1(M) − Control (M) and (bottom) N1(S) − Control (M). The shading interval is 1 hPa.

seeding and an SST anomaly similar to N1(M), proves that conclusion. This shows that increasing the seeding decreases the equatorward displacement of the storm track axis, basically reducing the feedback of the SST anomalies.

The results strongly suggest that

1) the variability of the quasi-permanent circulation could indeed be produced by the high-frequency eddy feedback; and
2) two main mechanisms operate for the forcing of the quasi-permanent circulation; *downstream development* from the western ocean and the anomalous *baroclinicity in the mideastern Pacific.* The intensity of these two counteracting forcings gives different flavors of the El Niño response over the PNA region. Note that the PNA patterns seem unique but obviously have different intensities regardless whether the SST anomalies are weak or strong.

Figure 20 presents a summary of the mechanisms controlling the response over the eastern Pacific Ocean for normal and enhanced tropical SSTs as just discussed. Although we did not specifically show cases with negative SST anomalies (La Niña conditions), it follows that a cold anomaly in the eastern tropical

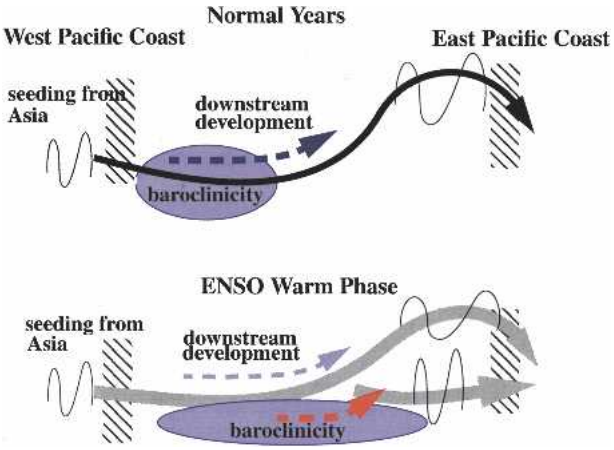

FIG. 20. A schematic presentation of the mechanisms that control the atmospheric response along the Pacific storm track, for normal and El Niño years. Solid arrows indicate the position of the upper-level jet; the wavy lines represent the eddies and indications of the change in horizontal scale for different regions along the storm track. Specifically, wavy lines on the extreme left depict waves entering from Asia, whereas wavy lines on the extreme right indicate the waves that characterize the high-frequency response at the end of the storm track. Note that on the subtropical branch of the storm track characteristic wavelengths are shorter than those on the polar branch. The blue areas represent the low-level baroclinicity that shifts to the east following the SST anomalies. The dashed arrows represent downstream fluxes enhanced by the pool of low-level baroclinicity. The blue arrow indicates fluxes emanating from the storm track entrance whereas the red arrow shows the enhanced flux due to the shifting of the baroclinic pool eastward.

ocean will further reduce the possibility of baroclinic development at these longitudes and enhance the effect of the building ridge in the PNA sector. These results suggest that perhaps combining methods that account for both the SST anomaly and the amount of eddy activity at the storm track entrance could significantly improve our ability to better predict the interannual response over the PNA sector. However the lack of predictability of the upstream seeding could limit the predictability of interannual variability over the PNA sector.

Acknowledgments. I would like to thank Isaac Held for the useful comments that helped clarify the manuscript and to Tom Knutson for the thorough review of the paper. I am grateful to Steve Garner for his efforts in developing the ZETAC model used in this study. Finally I would also like to thank Larry Polinsky for editing the manuscript and to Remik Ziemlinski for creating the display for the snapshots shown in the appendix, to Chris Kerr for providing valuable programming support, and to the GFDL Operations Staff that so efficiently scheduled the experiment runs. I would also like to extend my appreciation to the anonymous reviewers for the thorough review and comments on the paper.

APPENDIX

The Model and Maintenance of the Basic State

a. The atmospheric model

The ZETAC model (developed by S. Garner; more information available online at www.gfdl.noaa.gov/~io/Bubble.html) is a fully compressible nonhydrostatic atmospheric model developed at GFDL for regional weather and climate simulations. It uses an hierarchy of time steps (for acoustic–gravity waves, advection, physical parameterizations, and radiative forcing) to provide solutions for a wide variety of phenomena, from global (I. Orlanski and C. L. Kerr 2004, unpublished manuscript) to cloud resolving. It is now coupled, within the GFDL Flexible Modeling System, to component models of the ocean, land, and cryosphere. ZETAC uses terrain-following coordinates on a C grid. All experiments done for this study use open boundary conditions on the western (120°E) and eastern (85°W) boundaries. The model ran without radiative forcing or land–ocean model coupling, choosing instead to impose a reference wind and temperature profile through nudging at the western boundary. For this study we opted for the simplest micro physics package, namely, a Kessler scheme. Although the resolution could be variable, the simulation uses a $\frac{1}{4.25}$° ($\frac{4}{17}$°) horizontal resolution to achieve reasonable detail and affordable computer performance. However, for testing the convergences of our solutions to higher horizontal resolutions, we used a $\frac{1}{8.5}$° ($\frac{2}{17}$°) horizontal grid. A typical snapshot of both solutions is shown in Fig A1. The vertically integrated cloud water at $t = 10$ days is shown for both resolutions. The great detail that the clouds and mesoscale structure (at the $\frac{1}{8.5}$° resolution) exhibits is striking. The overall large-scale cloud patterns are quite similar. The similarity extends not only to the extratropical systems that seem to be controlled by the synoptic phenomena, but also to the deep tropical systems (see the southwest corner). These results are consistent with new simulations (O. M. Pauluis 2003, personal communication) for the tropical atmosphere with the ZETAC model and cloud-resolving scales. Recent experiments for 2-, 4-, and 8-km horizontal resolutions tend to show that the probability distribution function of vertical velocity is quite different in the tails; the 2-km resolution reaches the highest velocities. However, the rest of the distribution seems very similar for all resolutions. In conclusion, we do not know for certain if the midlatitude eddies will be affected by higher horizontal resolution and consequently the feedback to the larger scale because it is quite computationally prohibitive.

b. Maintenance of the basic state

Near the upstream (western) boundary, placed in this presentation at longitude 120°E, the basic state is main-

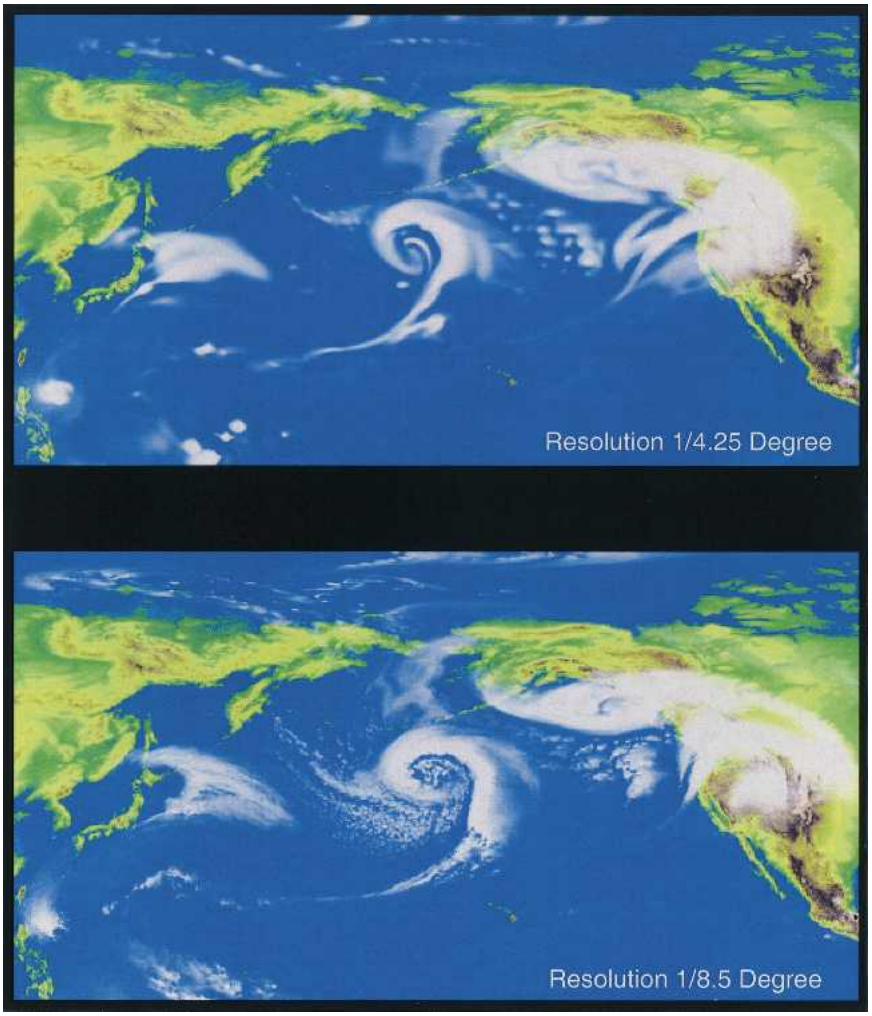

FIG. A1. Two snapshots of the Control simulation with two different resolutions, $\frac{1}{4.25}^\circ$ and $\frac{1}{8.5}^\circ$ horizontal resolution. Integrated column liquid water is shown.

tained by Newtonian damping within a sponge region that is approximately 3° wide. This appears sufficient to maintain a region of baroclinicity in which eddies can begin to develop. Traditionally, the basic state is maintained by zonally symmetric interior forcing. This approach is not adopted here so that the interior solution can freely respond to the eddy forcing. Instead, the sponge maintains a flow at the upstream boundary similar to the subtropical jet, a feature commonly observed at the entrance of the storm track. Consequently, these experiments do not represent the true large-scale variability in which storm tracks are embedded, but rather they can be used to examine the mutual dynamical feedback between baroclinic eddies and the quasi-permanent circulation.

c. Open boundary conditions and seeding

The so-called open boundary conditions in the ZETAC model are similar to the standard scheme (Orlanski 1976). Basically the scheme decides at each time if a point at the boundary is inflow or outflow. At inflow the variable is set to the previous time, whereas at outflow the variable is extrapolated. The inflow/outflow condition is decided by the numerical phase velocity, computed each time at a neighborhood of the open boundary only. This test is done on one variable only; in this case, it is the zonal wind. The condition is then applied to all the other variables. This open boundary condition has been used for many years in different kinds of (atmospheric and oceanic) models with considerable success.

In addition to the maintenance of the basic state by the sponge, there is a continuously perturbed meridional velocity variation nudged at the western sponge. The velocity perturbation changes sinusoidally with a frequency and amplitude that is randomly prescribed. After a random period oscillation finishes, a lookup table provides for an oscillation with a new random

period and amplitude (see Fig. 5). The vertical and meridional structure of the nudged perturbation is similar to that prescribed for the zonal jet to portray an upper-level wave entering the storm track.

REFERENCES

Chang, E. K. M., 1993: Downstream development of baroclinic waves as inferred from regression analysis. *J. Atmos. Sci.,* **50,** 2038–2053.

——, and I. Orlanski, 1993: On the dynamics of a storm track. *J. Atmos. Sci.,* **50,** 999–1015.

——, S. Lee, and K. L. Swanson, 2002: Storm track dynamics. *J. Climate,* **15,** 2163–2183.

Geisler, J. E., M. L. Blackmon, G. T. Bates, and S. Muñoz, 1985: Sensitivity of January climate response to the magnitude and position of equatorial Pacific sea surface temperature anomalies. *J. Atmos. Sci.,* **42,** 1037–1049.

Haltiner, G. J., and R. T. Williams, 1979: *Numerical Prediction and Dynamic Meteorology.* 2d ed. John Wiley and Sons, 477 pp.

Held, I. M., S. W. Lyons, and S. Nigam, 1989: Transients and the extratropical response to El Niño. *J. Atmos. Sci.,* **46**, 163–176.

——, M. Ting, and H. Wang, 2002: Northern winter stationary waves: Theory and modeling. *J. Climate,* **15,** 2125–2144.

Hoerling, M. P., and M. Ting, 1994: Organization of extratropical transients during El Niño. *J. Climate,* **7**, 745–766.

——, and A. Kumar, 2002: Atmospheric response patterns associated with tropical forcing. *J. Climate,* **15,** 2184–2203.

Kumar, A., and M. P. Hoerling, 1997: Interpretation and implications of the observed inter-El Niño. *J. Climate,* **10,** 83–91.

Kung, E. C., 1977: Energy sources in middle-latitude synoptic-scale disturbances. *J. Atmos. Sci.,* **34,** 1352–1365.

Kushnir, Y., W. A. Robinson, I. Bladé, N. M. J. Hall, S. Peng, and R. Sutton, 2002: Atmospheric GCM response to extratropical SST anomalies: Synthesis and evaluation. *J. Climate,* **15,** 2233–2256.

Lau, N.-C., and M. J. Nath, 1991: Variability of the baroclinic and barotropic transient eddy forcing associated with monthly changes in the midlatitude storm tracks. *J. Atmos. Sci.,* **48,** 2589–2613.

Madden, R. A., 1976: Estimates of the natural variability of time-averaged sea-level pressure. *Mon. Wea. Rev.,* **104,** 942–952.

Orlanski, I., 1976: A simple boundary condition for unbounded hyperbolic flows. *J. Comput. Phys.,* **21,** 251–269.

——, 1998: Poleward deflection of storm tracks. *J. Atmos. Sci.,* **55,** 2577–2602.

——, 2003: Bifurcation in eddy life cycles: Implications for storm track variability. *J. Atmos. Sci.,* **60,** 993–1023.

——, and J. Katzfey, 1991: The life cycle of a cyclone wave in the Southern Hemisphere. Part I: Eddy energy budget. *J. Atmos. Sci.,* **48,** 1972–1998.

——, and E. K. M. Chang, 1993: Ageostrophic geopotential fluxes in downstream and upstream development of baroclinic waves. *J. Atmos. Sci.,* **50,** 212–225.

Palmer, T. N., and J. A. Owen, 1986: A possible relationship between some "severe" winters in North America and enhanced convective activity over the tropical West Pacific. *Mon. Wea. Rev.,* **114,** 648–651.

Pierrehumbert, R. T., 1984: Local and global baroclinic instability of zonally varying flow. *J. Atmos. Sci.,* **41,** 2141–2162.

Shapiro, M. A., H. Wernli, N. A. Bond, and R. Langland, 2001: The influence of the 1997–99 El Niño–Southern Oscillation on extratropical life cycles over the eastern North Pacific. *Quart. J. Roy. Meteor. Soc.,* **127,** 331–342.

Simmons, A. J., and B. J. Hoskins, 1979: The downstream and upstream development of unstable baroclinic waves. *J. Atmos. Sci.,* **36,** 1239–1254.

——, J. M. Wallace, and G. W. Branstator, 1983: Barotropic wave propagation and instability, and atmospheric teleconnection patterns. *J. Atmos. Sci.,* **40,** 1363–1392.

Smith, R. K., 1969: On the effects of vorticity entrainment in zonal jet flows. *J. Atmos. Sci.,* **26,** 1233–1237.

Trenberth, K. E., 1993: The different flavors of El Niño. *Proc. 18th Annual Climate Dynamics Workshop,* Boulder, CO, National Oceanic and Atmospheric Administration, 50–53.